DOI: https://doi.org/10.24297/ijct.v22i.9229

Patient-appropriate and patient-specific quantification: Application of biomedical sciences and engineering principles for the amelioration of outcomes following reconstruction of osteochondrotomy of the sternum to access the mediastinum

Gandhi, Harjeet Singh MD, FRCS, FRCSC, MSc (Biomed Eng.)

Orthopaedic surgeon, Clinical Assistant, Hamilton Health Sciences, Hamilton, ON, Canada

harjeetg52@yahoo.co.uk

Abstract

It is a fact that the morphology, physiology, and load-bearing activities of two patients are never identical. The normal allometric variations in regional anatomy, primary disease processes, and co-morbid pathologies demand individual treatment planning and selection of implants for surgical repair, reconstruction, and replacement leading to patient-specific and patient-appropriate interventions. It requires quantification of hard and soft tissues of human anatomy directly or indirectly from image data and other evaluation techniques, which can be combined with reconstruction implant/s to form a composite structure for pre-operative evaluation.

Finite element modeling and analysis are routine engineering methods to assess the safety and endurance of the physical structures, which can be applied for the numerical evaluation of fracture/osteotomy reconstruction. The present study delves into the fundamentals of various imaging techniques and techniques for the acquisition of hard and soft tissue densities to extract material properties and introduces the practice of finite element methods for higher analysis and their intended surgical application.

Keywords: Sternotomy, finite element analysis, bone density, elastic modulus, elastography, fractals, fractal-like, clinical biomechanical engineer

Short title: Patient-appropriate and patient-specific quantification

Introduction

1.0 Patient-specific and patient-appropriate medicine

There are numerous terms such as "personalized medicine," and "precision medicine," to describe individual patient management in the context of genes and patients' clinical data. The shift in terminology reflects the collective demand of the scientific community based on progress in biomedical sciences. Generally, the term "patient-specific" implies customization to the precise anatomy, physiology, or holistic health care needs of a single person. In many patients' specific treatment strategies are developed on this all-inclusive definition, which often comes with potential sources of errors at all levels of patient care due to a lack of precise collection of clinical data, a variety of investigational procedures, and less considered patient-to-patient lifestyle variability. Frequently, it is recommended to support the management of a patient along with evidence-based medicine outcomes, which come with population-based statistically manipulated extraneous data, physician expertise, and patient preferences. The same can be said of a computational modeling pipeline in biomechanical engineering if one or more included parameters originate from cadaveric biomechanical experiments and a library of image-based data. An investigational technique and surgical technique can only be called *'patient-specific'* if the collected set of data specifically belongs to the same individual. In other words, the individual's data is without the inclusion of any kind of extraneous experimental or statistically averaged values based on anthropometric population data(Kent & Hayward, 2007).

The meaning of the term *patient-specific medicine* is neither synonymous with the above-mentioned terms nor interchangeable with *patient-appropriate medicine*. 'Specific' refers to something customized and precise, and 'appropriate' means that something is suitable and favourable to the special requirements, not simply to normal physiology, but in response to comorbid conditions as well. To apply mathematical assumptions in higher analytical calculations or say approximately is inaccurate and imprecise, because it may not be nearly so to the real values for surgical application.

In surgical practice, the objectives of *patient-specific medicine* relate to preoperative planning for developing treatment strategies, surgeon-based optimal selection of surgical approach as applied to a particular section of an anatomical segment, and applicable implants to mitigate intraoperative setbacks and postoperative complications to enhance the predictability of the patient-based outcome. To be more precise, the term *patient-specific* in the management of fractures and osteotomies, including osteochondrotomy of the sternum, be limited to a section such as the head, the shaft, or the condylar end of an index long bone segment of the skeleton under surgical intervention. Therefore, the *patient-specific* activity must appertain to a definite section of a particular segment of the human anatomy within an organ system having specific characteristics that are being isolated for qualitative and quantitative evaluation to acquire precision data in a definite manner for clinical application. There can be significant three-dimensional variations in the anatomical features such as surface contours, geometric dimensions, cortical and trabecular structure, effective muscle loading conditions, digital image quantification for bone mineral density, and bone material properties for numerical analysis to develop fracture/osteotomy reconstruction strategies.

An anatomical segment or organ under treatment is continuously influenced by the entire physiological and pathological interior milieu state of an individual patient. Therefore, the influential factors must be taken into consideration when a treatment plan is instituted, to expect a globally successful outcome of the treatment. This holistic principle is the foremost tenet of what here is referred to as *patient-appropriate medicine*(Gandhi, 2019) that can directly or indirectly affect native *patient-specific* quantitative biomechanical parameters. A patient coming for coronary bypass surgery who is due for an osteochondrotomy of the sternum frequently suffers from multiple co-morbidities such as diabetes mellitus, chronic obstructive pulmonary disease, high body mass index, renal insufficiency, metabolic bone disorder, etc. The female population with high BMI has large breasts that may produce excessive inferior and lateral postural distraction forces on the healing sternum and may become the cause of delayed healing, wound breakdown, and deep retro-sternal infection.

The rationale for directing effort towards *patient-specific* and *patient-appropriate* measurements are anthropometric variations of the human body in different geographical locations and subtle environment-dependent evolution. There are growth and developmental differences that depend on variations in socioeconomic standards and birth-related abnormalities. During development, there are proportional sex-specific allometric changes such as shape, size, form, and material properties over a lifetime. There are also variations in the pattern of the same disease and a variety of associated co-morbidities in the same patient at different times. For computer modeling of the sternum, there is a need for comprehensive geometrical measurements of all the dimensions – length, width, and thickness of the sternal components at various levels in relation to the costal cartilages, its sagittal plane curvature, and thoracic cage volume for optimization of patient-specific reconstruction implant that has suitable design parameters to meet the patient-appropriate requirements.

In clinical practice, there are several methods, such as plain radiography, computed tomography (CT), magnetic resonance imaging (MRI), etc. for the acquisition of 2D and 3D digital images for morphometric quantification. There had been increasing efforts with some success to deduce material properties of bone and soft tissues from image characteristics during in-depth image processing. The method chosen depends on the field of application, cost, and most importantly amount of radiation to the patient. Although the quality of data collection is dependent on the sophistication of the technique to provide 3D reconstruction automatically of the anatomy under examination it should also be cost-effective and made available swiftly. To attain the objective of constructing the computer model of a section or a complete bone segment for surgical application, the present study explores conventional chest radiography and the fundamentals of various other imaging modalities for obtaining hard and soft tissue densities to extract material properties and introduces the practice of finite element methods for higher analysis routinely

2.0 Inclusion of hard and soft tissue structures in the model

Based on the anatomy of the sternum (manubrium, gladiolus, and xiphoid) various geometric points can be defined to collect morphological data. Other than the 3D anatomy of the entire thoracic skeletal cage for finite

element modeling (FEM) there is a need for a greater understanding of the physiological reaction to the kinematics and forces acting on it for subsequent finite element analysis (FEA). In this respect, it is critical to consider the inclusion of other anatomical structures, including articulations, joint capsules and ligaments, extrinsic fascio-cutaneous coat, muscles, and even diaphragm to represent normal and abnormal respiratory movements. Depending on the volume of the breast tissue mass and posture of the person its weight may contribute significant traction force on the sternum directly via pectoralis major.

Anthropometric data can be collected by using standardized geometric points on the sternum and remainder of the thoracic cage anatomy, and salient soft tissue points. There can be inherent sources of error, particularly when it comes to measuring curved anatomy of the ribs and irregular structures constituting vertebral column from two or more views of 2D plain radiographs of the chest for 3D volumetric transformation following segmentation of skeletal anatomy of the thorax. Once a satisfactory 3D rendering of the thoracic skeleton with salient soft tissue structures is created, then only it is ready for finite element meshing of the model leading to a mathematical solution by applying patient-specific bone and soft tissue material properties and patient-appropriate loading and boundary conditions. For surgical precision applying population and the literature-based values would provide less than optimal bone-implant interface and response to the applied load. Although it is less than likely to fail, however, if it does, the participating clinical biomechanical engineering team carrying out the finite element analysis and making recommendations will face disappointment, lose the trust of the surgeon, and from the health provider's prospective investment in tools and time.

3.0 Digital imaging and current chest radiographic techniques

3.1 Review of digital image properties

Medical images are a 2D representation of 3D physical structures of normal or pathological human anatomy. They are heterogeneous in appearance even within the same anatomic region. Almost all medical images are packed with multiple regions of varying tissue densities depending upon the hierarchy of cellular structure constituting the tissues, and the amount of air, water, and mineral content. As x-ray imaging is an energy attenuation modality the projected pixel grey-level values in the image represent tissue densities depending upon the amount of x-ray beam attenuation when transmitted through each tissue constituting the region. By convention, the denser the tissue brighter the representation in an image(GEOFF DOUGHERTY, 2009). Thus, the various structures in a busy image like a chest radiograph can only be recognized easily because of the varying pixel intensities of the tissues. In comparison to ionizing radiation-based computed tomography (CT), plain radiography differentiates fewer tissue densities. Whereas magnetic resonance imaging (MRI) based on absorption and emission of the radio-frequency wave is related to the applied sequence (T1 and T2 weighted images) in a high-power magnetic field. Therefore, the image intensities seen on MRI do not correspond to the image intensities resulting from x-ray attenuation equivalent to tissue densities as projected in radiation-based images of the same region.

3.2 Conventional chest radiography –

The standard image of the coronal posterior-anterior (PA) view of the chest radiograph is to examine soft tissue structures in the thorax. The projected x-ray beam is attenuated in variable amounts when transmitted through the chest as there are high-density bones, cartilage tissue, soft tissues, blood in the heart and vessels, and air in the lungs. The real-world 3D anatomic structures projected in the image are superimposed and 'compressed'. The observing physician must merge the orthogonal views in his or her mind to realize 3D anatomy to extract in-depth meaningful information.

The bone has a higher attenuation coefficient than soft tissue because of greater photoelectric absorption. However, the radio-dense heart attenuates most of the photoelectric beam absorbing the greatest number of the x-ray photons, so that in a PA view the sternum is completely occluded by it. If the thoracic spine is not visible in the silhouette of the heart it means the image is underpenetrated. The advantage of the digital imaging technique is that the appearance of images can be improved to distinguish various structures, the image information can be stored and processed, and used for higher numerical analysis by building a 3D anatomy model. As the objective of chest radiography is to delineate soft tissue structures rather than the thoracic skeleton, special views are required to image structures of interest that are either occluded or lost due to

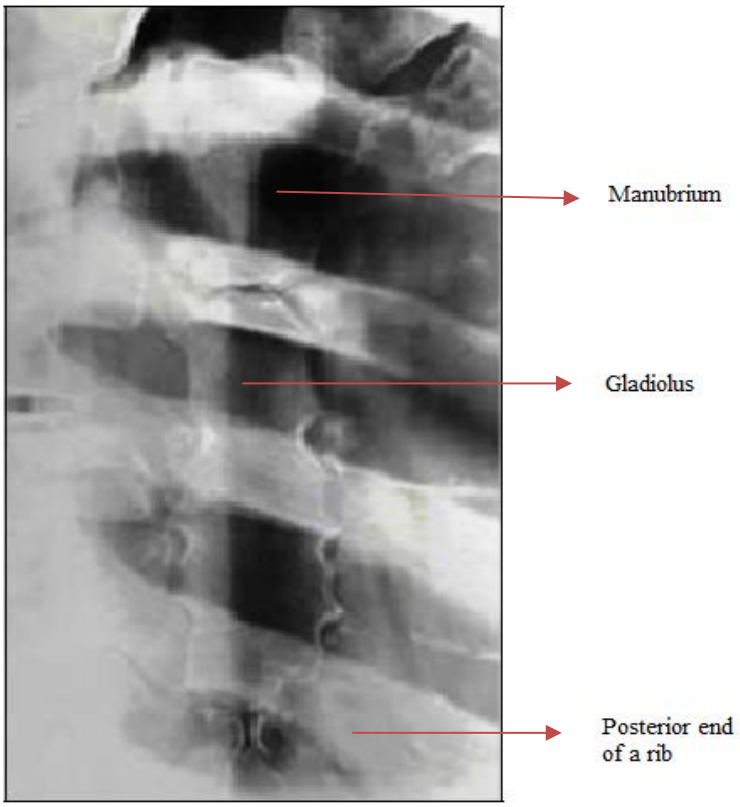

Figure 1– A section of the right anterior oblique view of the chest x-ray to demonstrate the coronal view of the sternum from behind. The image has been modified to enhance its appearance for clarity. The problem of altered grey-level values of the sternum due to the overlapping of other tissues to calculate the real tissue attenuation density of the sternum is obvious in a multilayered image like that of the thorax. (Source - xrayandradiologylecturenotes.blogspot.com/2012/12/sternum-clavicle-ribs.html).

overlapping structures averaging overall tissue density represented in the form of equivalent pixel intensities. The sagittal anatomy of the sternum is visible adequately in the lateral view. To see its anatomy in the coronal plane generally a 20-45 degree anterior oblique x-ray beam is directed at the sternum to pass through the paravertebral plane (Fig. 1). The shadow of the sternum rests on the heart silhouette or radiolucent lung depending on whether the right or left anterior oblique view is taken. A reasonable quality coronal image of the sternum is produced with overlapping posterior rib shafts. In all the views of the chest, there is overlapping of the structures, which makes recognition and counting of the ribs difficult to label for application of point markers during the integration of the 2D radiographic views for 3D reconstruction of the thoracic cage.

3.3 Dual-energy subtraction chest radiography

The variation in tissue densities resulting in different degrees of x-ray beam attenuation is central to the development of the dual-energy subtraction radiographic technique. Bone absorbs a greater number of photons as it has a higher atomic number of calcium atoms relative to soft tissues(Vock & Szucs-Farkas, 2009). It means by projecting x-ray beams of two different energies, simultaneously or separately with a high degree of attenuation differential can help separate structures of high and low photon absorption tissues. Thereby, manipulation of energy differential and image contrast of either bone or soft tissues can be enhanced to isolate higher-density bones from lower-density structures(Brody et al., 1981). The higher photon attenuating bone tissue is the result of a low-energy beam. The effective x-ray beam energies generated for the dual-energy subtraction process are 60kVp and 120kVp. The two images captured at these different energies are weighted relative to each other, and at the time of image decomposition if the high-energy weighted image is subtracted by bringing its signal to almost zero, then only low energy weighted image structures are preserved; otherwise, both images are available for visualization separately. Total ionizing radiation exposure to the subject is about 15% more than PA and lateral views of standard chest radiography(Vock & Szucs-Farkas, 2009).

3.4 Dual-energy digital tomosynthesis

In computed tomography, multiple 2D planar images containing 3D information are collected at the same time without altering the geometric parameters of the object, and the image coordinates to unify the information for the reconstruction of 3D anatomy. A similar computing strategy is employed to undertake the dual-energy tomosynthesis imaging process. The initial orientation of the subject, the x-ray tube, and the flat-panel detector are like standard chest radiography. In dual-energy digital tomosynthesis, the relative motion of the tube and detector panel is pre-determined to bring the plane of the desired location in constant focus(Dobbins et al., 2008).

As the technique is based on the dual-energy subtraction principle the tomosynthesis system uses 60kVp and 120kVp x-ray projection beams for imaging the thoracic cage in posterior-anterior orientation. Unlike CT, where the x-ray beam takes a spiral path to strike multiple detectors as the gantry translate, here multiple scans are obtained by making a single sweeping motion of the tube through a pre-determined rotation angle (35-40 degree) to include the entire field of interest. The collected set of multiple low and high-energy image slices are reconstructed to generate a much higher quality image compared to the dual-energy subtraction technique. The motorized movement of the tube is controlled by a computer program along a vertical linear path to acquire projected images on a single flat panel detector(Dobbins & McAdams, 2009). By applying a weighted subtraction program bone or soft tissue tomograms can be produced depending on attenuation co-efficient differential.

Although digital tomosynthesis does not provide as good depth as seen on the CT, it is cheaper, produces much higher quality images than conventional chest radiography, and has the advantage of low radiation dose exposure. In a multi-centre prospective randomized study to compare dual-energy subtraction, digital tomosynthesis, and conventional chest radiography trial, the relative effective clinical dose for conventional chest x-ray was 0.02-0.19mSv; digital tomosynthesis was 0.07-0.41mSv, and for CT was 1.4-18.2mSv(Dobbins et al., 2017).

3.5 Electronic optical system

Both CT and MRI techniques lend well to reconstructing 3D virtual structures with the help of incorporated software, but they have individual limitations. Alternative to these is a new research technology called electronic optical system EOS®. It has a set of two orthogonally arranged x-ray beam heads in the calibrated environment, which provides 3D reconstructed images of a region. As most of the work done is to study scoliosis, it excludes the sternum and like all known x-ray modalities it also does not show the costal cartilages. The system is synchronized to take posterior-anterior and lateral views at the same time, reducing the radiation dose to the patient. It comes at a very high installation cost with system-specific limitations and cost-effectiveness(Melhem et al., 2016) and limitations of the 3D virtual model for precision surgical work(Glaser et al., 2012).

So far there is no known suitable low ionizing radiation technique that can be applied safely and rapidly for the reconstruction of a 3D virtual model of the thoracic skeleton for higher numerical analysis for surgical intervention. Among the techniques discussed above, standard PA, lateral, and right or left anterior oblique chest radiographic views are simple and fall within the everyday experience to construct a 3D stereo radiograph of a complete thoracic skeleton. However, it is worth considering dual-energy subtraction and tomosynthesis techniques as they make the production of higher-quality images and segregation of the thoracic skeleton possible.

This study also proposes the acquisition of the 3D structure of the radiolucent costal cartilages by exploring the worth of 3D volume rendering ultrasound technology to include them as they play a significant role in the biomechanics of the thoracic cage during respiration and when an external load is applied. Intercalation of patient-specific costal cartilage anatomy and availability of their original pixel intensities would help extract their elastic modulus for numerical analysis and surgical applications.

4.0 3D The role and ultrasound imaging of the costal cartilages

The costal cartilages play an important biomechanical role in the movements of the thorax, which is benignly ignored in both experimental and clinical practice. Whereas the investigative role of ultrasound in the examination of the chest wall is less described in literature than in computed tomography and magnetic

resonance imaging. The costal cartilages are projected neither on CT nor plain radiography of the chest unless ossified.

4 .1 Structure and biomechanical role of the costal cartilages

The first to seventh costal cartilages are intercalated between the ribs and the sternum, and the eighth to the tenth articulate with each other and ultimately to the seventh (Fig. 2 and Fig. 4). Except for synarthrosis between the first costal cartilage and the manubrium rest of the costo-sternal articulations are synovial, which means some movements must be occurring there. As embryonic structures, the continuation of the un-ossified costal cartilages into the bony ribs varies in length and the cross-sectional area(Standring, 2008). The extra-thoracic and intra-thoracic surfaces of the intercalating costal cartilages provide attachment to the muscles and contribute a significant amount of elasticity to axial rotation of the ribs(Standring, 2008), and act as torque bars to store energy for smooth motion of the sternum during respiration. The costal cartilages undergo an ossification process throughout adulthood, and it varies in amount and distribution in males and females(Stewart & McCormick, 1984). A definitive pattern is observed in the distribution of ossified areas, being peripheral in males and more central in females(Rejtarová et al., 2004).

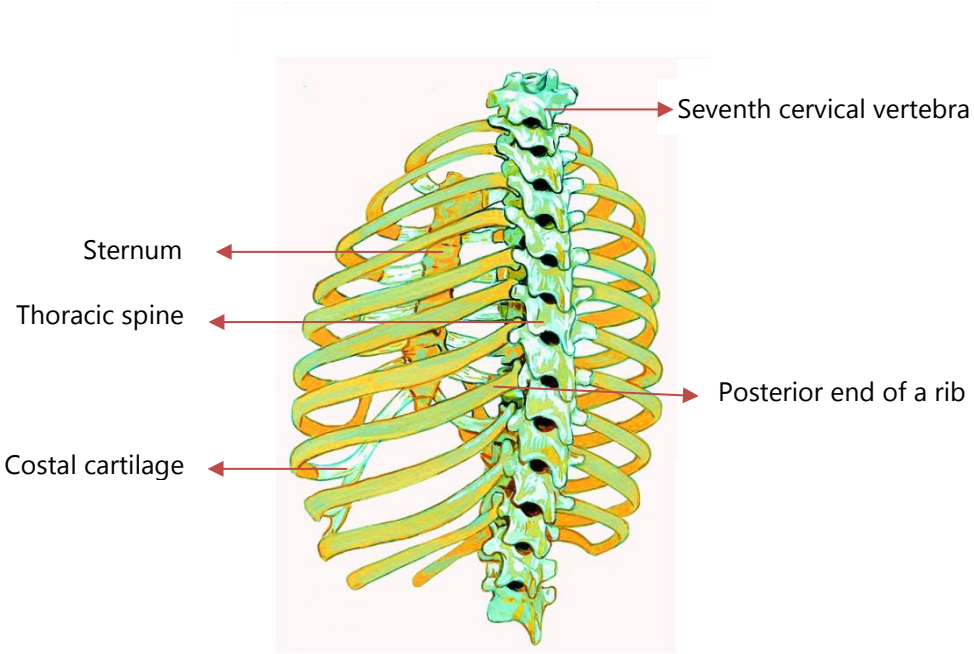

Figure 2 – Left posterior-anterior oblique view of the thoracic skeleton showing the posterior surface of the sternum through overlapping posterior rib shafts.

Although the biomechanical significance of the age-related ossification pattern of costal cartilages remains unexplained, the formation of the ossified shell overall provides 50% more stiffness to the structure of the chest wall(Murakami et al., 2006). The relative degree of volumetric increase in ossification results in an equivalent change in the elastic modulus of the costal cartilages(Oyen et al., 2005) with age-related growth and change in its geometrical shape. The reported elastic modulus measured by the indentation technique is between 5.5 and 14.2MPa(Forman et al., 2010; A. Lau et al., 2008). The costal cartilages lead to a global gender-specific change in the elasticity of the whole thoracic cage in response to an external load, as has been observed in age-related calcification at other hyaline cartilage sites(A. G. Lau et al., 2011).

It means for true patient-specific and patient-appropriate parameters for finite element modeling and analysis, complete 3D geometry and volumetric mineral density of the costal cartilages must be considered as it changes the behaviour of the model with a change in its material properties(Forman & Kent, 2011; Huang et al., 2019). Therefore, it becomes important that the biomechanical role of the costal cartilages is considered whenever patient-specific and patient-appropriate finite element analysis is planned for the sternum under normal and

pathological external loads. To achieve this goal, it is necessary to build a 3D structure of the costal cartilages and stitch it within the topographic anatomy of the 3D thoracic cage model.

4.2 Three-dimensional ultrasound modality

So far 3D ultrasound for volume rendering of costal cartilages has not been explored very well, however, it has been applied to study parts of thoracic and abdominal walls(Meuwly & Gudinchet, 2004) as a diagnostic tool(Battistelli & Anselem, 1993; Choi et al., 1995). It has also been used as a research tool to study the progress of fracture healing in the long bones to assess the 3D anatomy of radiolucent fracture callus(Nicholson et al., 2019; Wawrzyk et al., 2015). The 3D ultrasound imaging technique can study the 3D anatomy of the costal cartilages and has been successfully shown to demonstrate the injuries and other pathological lesions of the costal cartilages(Battistelli & Anselem, 1993; Choi et al., 1995). There are methods and systems available for rendering high-quality 2D ultrasound data to produce 3D volumetric images(Mozaffari & Lee, 2017). The acquired scanned data and corresponding geometrical orientation of multiple image slices containing sectional anatomy information are computed to render 3D ultrasound volume. The 3D surface model from 2D images in anatomic order is stacked to construct a 3D voxelized volume in x, y, and z-axis space(Fenster & Downey, 1996). The missed-out sections of the anatomy due to errors in sweeping and tilting movements of the transducer are computed by interpolating grey-level values of the available pixels and voxels in the stack. To extract specific region-of-interest 2D images are mapped, segmented, and interpolated to reconstruct 3D structures with the help of available software(Prager et al., 1999).

With the acquisition of all the bony and cartilaginous elements of the thoracic skeleton, it will be possible to reconstruct and animate rendered 3D virtual model. It will allow the operator to interactively visualize complete anatomy from different perspectives and after finite element analysis observe representative stress and strain variations on the von Mises map.

5.0 Stereo-radiography process for 2D to 3D reconstruction

The 2D images come with a loss of depth, which is represented along the z-axis. To reconstruct 3D images from 2D images require two or more views taken in coronal, sagittal, and one or more oblique views to acquire maximum information about the shape, size, and orientation of the normal anatomy and the pathology embedded in it.

5.1 Current state of 2D to 3D reconstruction

There are numerous techniques described in the literature based on statistical shape modeling, parametric and geometric deformable models, and feature-based methods(Goswami & Kr., 2015; Hosseinian & Arefi, 2015). Broadly speaking, in these techniques, some methods use only one or two plain radiographs as input views merged by solving mathematical algorithms. The statistical shape modeling requires many examples to build a training set of atlases(Dworzak et al., 2010) and in the case of the template method, the 3D model is used to reconfigure calibrated x-ray images of a given patient by elastic deformation using a non-stereo corresponding contour algorithm(Laporte et al., 2003). The feature-based methods employ point cloud which requires the skills of an expert operator to identify salient anatomical points and lines manually on all the radiographic views(Zheng G, Gollmer S, Schumann S, Dong X, Feilkas T, 2009). The point cloud method is preferable because of its simplicity but it is labour intensive and involves the cost of a dedicated expert.

5.2 Photogrammetry and direct linear transformation

The stereo-radiography employs the basis of the stereo-photogrammetry algorithm and direct linear transformation for stereo correspondence of selected points on the input views(Aubin et al., 1997; Dansereau & Stokes, 1988). It combines two or more views taken simultaneously or one at a time from different positions of the same type of imaging system or different poses of an object or a subject with a single system if the coordinates of all the views are constant. The photogrammetry process is to record, measure, and interpret real-world photographic information to generate three-dimensional image data (stereo-photogrammetry) to produce 3D digital models of 2D images (Fig. 3). The object in 3D real-world space and 2D image plane captured by two or more digital cameras or radiography imaging systems are calibrated to establish the same Cartesian coordinates of the object and the image space.

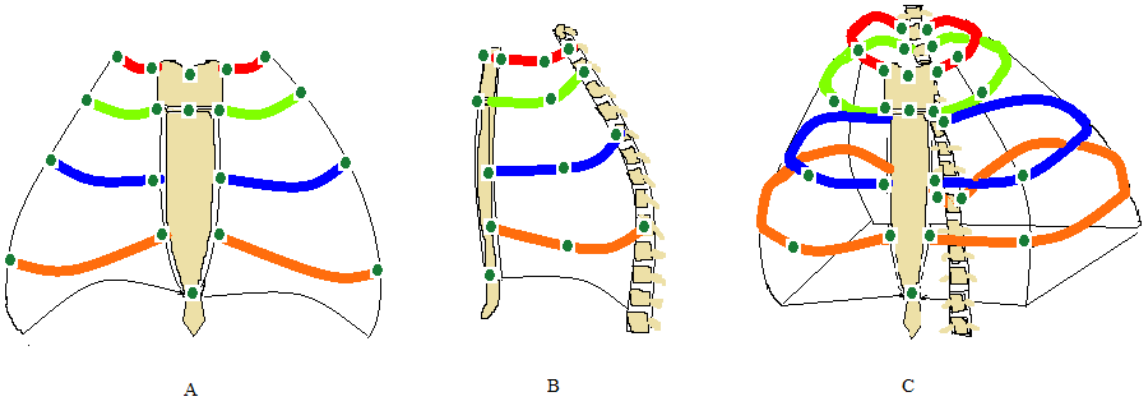

Figure 3 – A simplified line drawing to demonstrate the process of the stereo-photogrammetry process to reconstruct 3D skeletal anatomy from two 2D plain radiographic views. **A.** anterior view and **B.** lateral view with skin markers placed on salient features, and **C.** reconstructed 3D anatomy following stereo correspondence of "point clouds" by applying the direct linear transformation.

The radio-opaque markers placed on the skin surface of a patient or placed in the outside space for calibration are kept common to all the views. In all the images of various views, the coordinates are applied to each point on the selected salient features of anatomical structures. The photogrammetry algorithm(Dansereau & Stokes, 1988) is applied to minimize the distance between similarity points in all the views by what is called the sum of the squares of errors within coordinates relative to the displacement of all the reference points. While the stereo-photogrammetry estimates the 3D coordinates of all the included points used as markers on a 3D object and the same points are measured on all the views taken from different fixed positions in space(Rajulu, S Corner, 2013). For stereo correspondence, salient anatomical points are marked manually using radiographic markers. The radio-opaque skin markers are identified on radiographic views to integrate the images into single 3D coordinates equivalent to 3D space. As all the arrangement including 3D anatomy, imaging modality positioning, and skin markers is manual, therefore, to unify all these into meaningful data each item must relate to each other constantly during the acquisition of all the views, to replicate the 3D object into a symmetrical 3D end-product.

The constancy of calibration is imperative to resolve geometrical equations between the points in all the views to establish co-linearity with the direct linear transformation method. Therefore, the calibration of radiographic imaging modalities is preferably achieved by placing one or more skin markers on the region of interest (Reinhard, 2014). In case there is a single imaging system, as generally is the case for a standard chest x-ray, then the synchronization process is a significant step when taking multiple views to produce a meaningful high-quality 3D model. It is the direct linear transformation program that optimizes the correspondence of the anatomic points(Dansereau & Stokes, 1988). Mathematically, there are unknown terms in the linear transformation matrix for calculation for each point(Reinhard, 2014). The radio-opaque skin landmarks and the paired points marked on the images are converged iteratively until the co-linearity distance between them is less than 0.1mm(Dansereau & Stokes, 1988). Thus, the 3D virtual image is generated as discrete points on all the matched views. The rigours of the technique are to apply the algorithm to all the points and compute them with the help of a software application.

In summary, stereo-radiography involves two or more radiographic views representing region-of-interest and calibration of the imaging modalities to match object space to image planes for constancy of coordinates. Then carefully maximum numbers of anatomical features are selected to mark points on the regional anatomy, followed by the application of a photogrammetry algorithm and direct linear transformation program for stereo correspondence of points to integrate all the views into 3D anatomy. At the time of calibration, a constant geometric relationship between the subject and the two or more radiographic imaging modalities is highly desirable to prevent the reflection of errors in the final 3D reconstruction for precision surgical applications. The

technique demands complex mathematical formulations to reach desirable accuracy particularly when it is applied for the insertion of pedicle screws in corrective surgery of a scoliotic spine.

Before imaging, the radio-opaque skin markers less than 1.0mm in diameter are applied at the centre of the sternal notch, junction of manubrium-gladiolus, and gladiolus-xiphisternum in the sagittal plane for calibration between the subject and the imaging modality in all the planes. Additional markers on the ribs, mid-shaft of both the clavicles, posterior and anterior elements of the thoracic spine, and spinous process of the seventh cervical vertebra, and many more sites on the 2D images are selected to increase the precision and quality of the final reconstructed image (Fig. 4). The calibration and additional markers are used for the photogrammetry algorithm and the direct linear transformation program.

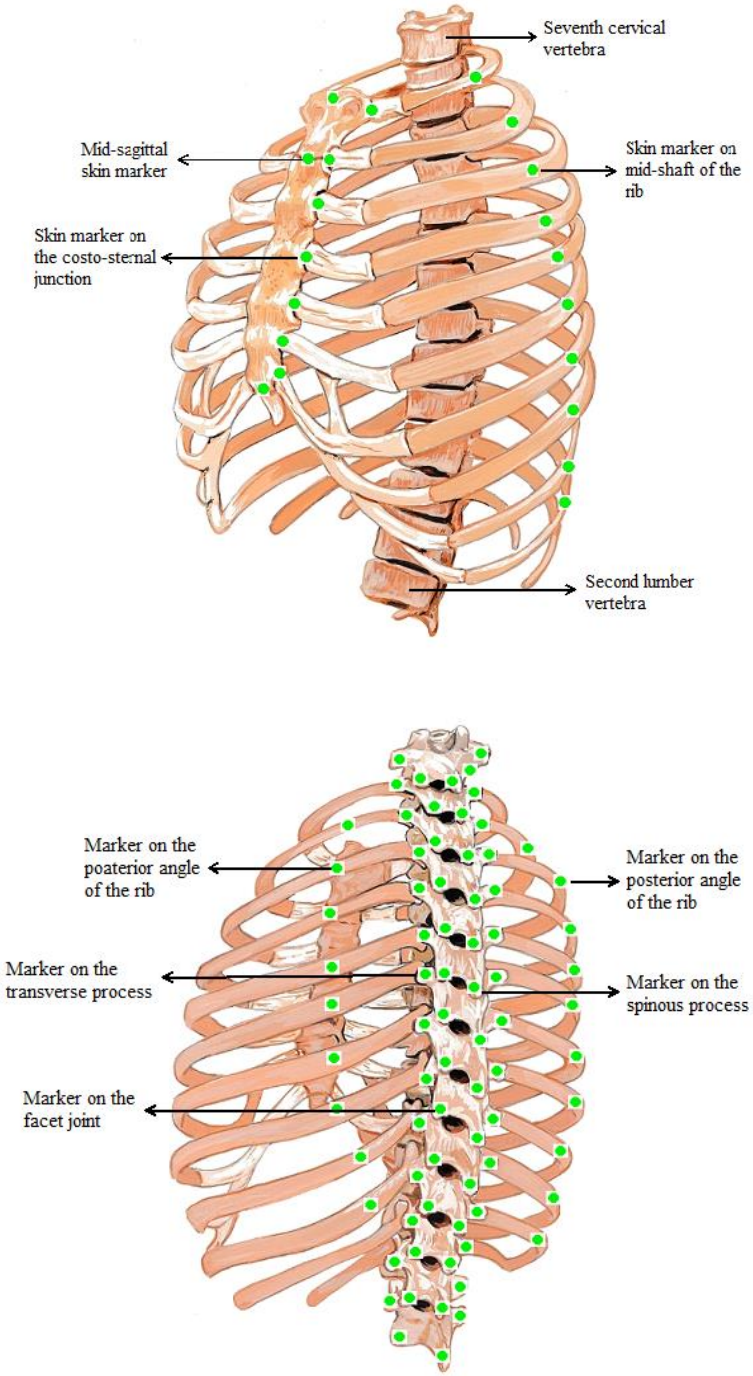

Figure 4 – Suggested skin and additional markers on the x-ray images shown on oblique anterior-posterior (top) and posterior-anterior (bottom) views of the thoracic skeleton for plain radiographic imaging.

6.0 Image-based bone density and material properties of hard and soft tissues

Developing a patient-specific clinically valid engineering bone model with or without an implant requires the geometry of the skeletal segment, bone density of the specified section of the skeletal segment, material properties; boundary conditions, and patient-appropriate loads to calculate the stress and strain values in each bone. Hence, the measurement of bone density and extraction of the bone material properties for patient-specific application is one of the fundamental roles of medical image analysis and image processing. Mechanically, in the living, the wet bone is almost a solid composite structure. How it responds under load is dependent on bone strength as the function of bone mineral content per unit volume of the bone tissue. And the way the mineral is distributed at a specific site in its 3D anatomy accounts for local bone density. At any given site, in addition to the bone geometry, it is the local bone density and orientation of the collagen fibres that confers upon bone its global material properties to resist applied forces.

To choose the most ameliorative patient-appropriate implant design the skeletal segment primarily requires segregation by applying the most suitable segmentation method for analyzing patient-specific bone geometry and local density to calculate bone material properties such as elastic modulus for further analysis. The reconstruction of a 3D bone model from 2D plain radiographs or CT slices can easily provide bone geometry and bone density as Hounsfield units (HU) extracted from image intensity to calculate bone material properties.

Figure 5 – An x-ray image of the head and neck of an adolescent femur showing weight-dependent orientation and distribution of the trabeculae.

6.1 Radiation based measurement of bone density

Visually, a rough estimate of bone density and strength can be made from the thickness of the diaphyseal cortex and the lush distribution of trabeculae as stress lines in the metaphyseal zones on plain x-ray images (Fig 5). In elective surgery, to assess the fracture risk the bone mineral density (BMD) can be measured using radiation-based technologies such as dual-energy x-rays, quantitative CT, and less often ultrasound. Quantitative CT (QCT) is more sensitive for detecting osteoporosis than dual-energy x-rays(Adams, 2009). Dual-energy x-ray technique measures areal BMD in a 2D frame at specifically selected sites. It does not distinguish between cortical and trabecular bone mineral density. The guiding values are population-based standard deviations rather than patient-specific. On the other hand, QCT provides a 3D volumetric window to measure BMD against a calibrated phantom placed in the field. It differentiates between cortical and trabecular bone at the anatomical site of

interest and is more patient-specific(Kaufman and Siffert), 2001). Apart from cost, excessive radiation compared to dual-energy x-ray technique QCT is an ethical concern to assess a person for fracture risk, albeit important.

6.2 Fractal dimension and bone strength

Osteoporosis is a systemic disease characterized by low bone mass and deterioration of bone micro-architecture, leading to increased bone fragility and consequently an increase in fracture risk("Consensus Development Conference: Diagnosis, Prophylaxis, and Treatment of Osteoporosis," 1993). The image intensity has a high correlation to the amount of calcium in the bone. The higher the mineral content higher is the attenuation of x-rays and the higher the grey-level value. To relate the bone mineral content to grey-level values it is necessary to standardize radiographic images for further reliable analysis. The trabecular bone is built of variably dense interlacing micro-beams made of osteons within the cortical envelope to form a honeycomb structure of varying-sized lacunae to resist compression is an important architectural design feature that is used to assess bone strength(Dalstra et al., 1993; Mullender et al., 1998) in dentistry.

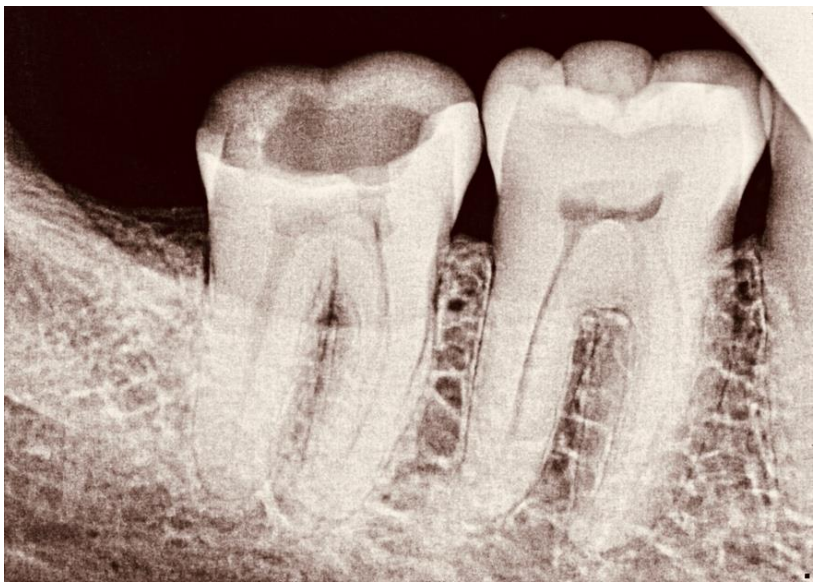

Figure 6 - A plain radiograph of the trabecular bone of the mandible demonstrating varied geometrical shapes and dimensions of the fractal-like structure of inter-trabecular spaces.

The technique of fractal dimension has been applied to study the characteristics of trabecular structure seen on plain radiographic images of cortico-cancellous bone of the mandible to measure its bone density (Fig. 6). A fractal is a geometrical structure when magnified or divided into smaller parts still retains its original shape referred to as self-similarity(Mandelbrot, 1983). In healthy bones, the fractal dimensions are smaller and there are more fractal boxes (intertrabecular lacunae) per unit area/volume, and the greater the number of thick trabeculae per unit volume higher is the bone mineral content(Harrar & Hamami, 2008). As the trabeculae get sparse in the case of osteoporosis the fractal dimensions get larger due to an increase in the size of lacunae with thinning and loss of the trabeculae. Although there is a close relationship between the number and the thickness of the trabeculae and the total grey-level value of pixel intensity and fractal dimension of a region due to the degree of x-ray attenuation, however, there seems to be no significant relationship with bone mineral density(Camargo et al., 2016). The fractal dimension of local trabecular bone may be considered when bone quality is being assessed for low-demand tissue anchoring implant surgery.

6.3 Calculating elastic modulus of the patient-specific bone segment

Bone is a heterogeneous composite material, and each skeletal segment responds differently to load depending on its unique geometry and bone density. In its natural state, the bone material is viscoelastic and anisotropic in-vivo and much of it may change during storage and preparation for experimentation(Turner & Burr, 2001) to estimate mechanical properties for clinical application. Therefore, the application of experimentally extracted

bone material properties is less than optimal and not patient-specific. It becomes even more irrelevant when approximate patient-appropriate loading conditions are applied for numerical analysis and surgical treatment. Secondly, under experimental conditions bone material is generally assumed to be homogeneous and isotropic, with a linear stress-strain relationship, which defies the ground truth in real life for a given patient.

The elastic modulus refers to the stiffness of engineering material and the relationship of stress-strain represents linearity up to the point where the deformed material will return to its original physical state, and beyond which it will sustain permanent plastic deformation. If the time-dependent repetitive load continues the material will yield, creating a stress fracture depending on strength of the material, which is related to bone density and its geometry. It has been now known for a fair length of time that there is a physical relationship between bone density and elastic modulus(Carter & Hayes, 1977; Helgason et al., 2008). There are several power laws to find elastic modulus from bone mineral density. One such power law to calculate the elastic modulus of bone is based on Morgan's material law(Morgan et al., 2003). The calculated result can be used for in-silico experimental finite element analysis of the bone with or without an implant. It has also been known that there is a significant correlation between CT image grey-level values and the apparent density of trabecular bone(McBroom et al., 1985). From the CT image, three bone density parameters are extracted – bone mineral content equivalent to grey-level values, bone ash, and bone ash mass(Schileo et al., 2008). And, CT numbers or Hounsfield Units (HU) is a quantitative radio-density scale, which has a linear relation to x-ray attenuation. Under the same conditions, distilled water has zero HU and air has minus1000HU. To obtain the value of HU the bone mineral content of wet bone specimen is first converted to the apparent bone density, which in turn is applied to Morgan's law to calculate elastic modulus(Keyak et al., 1994). According to Morgan's law $E = 6.95d^{app1.49}$ where E is Young's modulus in Giga Pascal and d^{app} is apparent bone density in g/cm^3. 3D image reconstruction of a bone provides a voxel-based image intensity gradient for bone density calculation and volumetric bone geometry including the cortical and trabecular architecture of the skeletal segment for finite element meshing and numerical calculation.

6.4 Elastography to extract mechanical properties of soft tissues

The skeletal muscles, skin, and subcutaneous fat around the thoracic cage, and the breasts over the surface of the chest in females form a major component of the soft tissue envelope. The amount of soft tissue and the action of the underlying muscles directly influences the stability of the healing osteochondrotomy of the sternum. Considering the weight of the soft tissue coat, the breasts and the forces generated by the active musculature, including the diaphragm, oppose the function of the fixation implants. Therefore, it is only reasonable to include the weight and material properties of these soft tissue structures at the time of FE modeling (FEM) and FE analysis (FEA). Although the elastic modulus values of these soft tissues are available from the literature but cannot be applied for patient-specific higher analysis.

There are few imaging techniques available for exploration to measure the elastic modulus of soft tissues. They employ physical principles of ultrasound, MRI, x-rays, and optic and acoustic signals, grouped under the heading of elastography(Sarvazyan et al., 2011). The soft tissues are considered "incompressible" because of the abundance of water, relative to contained solid organic materials. It means the application of external force changes the shape of the tissues depending on their elastic modulus, without altering their volume. Other related soft tissue parameters are the bulk compressional and shear elasticity moduli, which respectively depend on molecular composition and their interaction, and to structural architecture of the tissues(Savzyan AP, 2001). The Poisson's ratio (relative change in shape under load) of well-hydrated soft tissues is close to 0.5. For static deformation the reported shear elasticity modulus of soft tissues is approximately one-third of the elastic modulus and the bulk compressional modulus for all soft tissues is approximated to that of water, varying within 10% of it(Sarvazyan et al., 2011), likely dependent on the amount and distribution of solids in it.

Of all elastography techniques, the simplistic technique of strain ultrasound elastography for clinical application is based on Hooke's law. It can be used effectively to measure elastic modulus by applying direct compression adjacent to the region of interest for mapping the material properties and measured as the ratio of stress and strain, relative to a reference tissue such as adipose tissue. The compression can be either applied via the handheld ultrasound transducer or physiological movements generated during respiration in the case of the thoracic cage. The compression load can be variable and operator-dependent. Therefore, supersonic shear wave

imaging is preferred where ultrasound waves are generated within regional tissues by the same transducer that receives the reflected waves for assessment(Bercoff et al., 2004; Gennisson et al., 2010). It is the velocity of the transmitted shear waves, which is measured to calculate the elastic modulus ($E = 3 \times V^2$ kilo Pascal)(Bercoff et al., 2004).

The heterogeneity of the tissues within the same category, alignment of the probe, and the relative value of the elastic modulus between the mapped region-of-interest and reference tissue within an elastogram make it a comparative semi-quantitative parameter of dissimilar tissues, depending on operator choice. Secondly, when the overlying soft tissue coat on the muscles is thick the mean values acquired by manual force strain elastography of the deeper tissues may be less reliable as compared to shear wave elastography imaging. The most significant clinical advantage of elastography is that it is a non-invasive technique. Currently, despite limited clinical applications, the elastography technique may still be considered an important tool to measure in-vivo biomechanical properties of muscles(Levinson et al., 1995) for patient-specific and patient-appropriate FEA.

7.0 Patient-specific bone density and elastic modulus of the thoracic cage elements

The HU and bone density of the sternum can be measured reliably in all those patients who undergo cardiac CT to assess coronary artery calcification. The thoracic spine bone mineral density measurements recorded in the females are higher than the males (female 222mg/cm^3 and males 215mg/cm^3) and are 17-20% higher than the lumbar spine when measured with QCT ($p<0.001$)(Budoff et al., 2010). The literature is silent on the areal bone density measured with the dual-energy x-ray of the sternum in-vivo because it is concealed by the thoracic vertebral column and blanched out by the cardiac shadow. In a cadaveric study, the bone mineral density was determined by measuring the bone ash method the male sterna were found to be denser than the female in all regions of the sternum and central mid-line density was higher than along the lateral edges(Selthofer et al., 2010). The reported bone mineral density of the manubrium ranged from 169 to 220mg/cm^3 and for the gladiolus it was 160 to 227mg/cm^3. Statistically, there is a significant age-related reduction of bone density in the sternum of the females than the males, thereby increasing the risk of fracture during surgical retraction and dehiscence following osteochondrotomy of the sternum. How insignificant the statistical differences may seem to be between the living and the cadaveric values, there are significant differences in inter-regional and intra-regional values of bone mineral density when it comes to developing a site-specific and a *patient-specific* FEM of a whole bone to measure the outcome of locally applied loads under an implant in a *patient-appropriate* surgical application.

The correlation between elastic modulus and grey-level pixel and voxel values are given in the literature(Reeves et al., 2012; Viceconti et al., 1998) cannot be compared because the studies lack consistency in methodology, standardization of imaging modalities to extract image intensity gradient, vary in choice of anatomical sites, and are population-based. There are also intra-region variations in the estimated elastic modulus. For example, the elastic modulus values vary between anterior (7.5GPa), lateral (11.9GPa), and posterior segments (10.7GPa) of a rib ($p<0.01$)(Stitzel et al., 2003). The literature has limited studies on the material properties of muscles and is silent on the correlation between grey-level values and material properties of soft tissues directly related to the skeletal system for inclusion to optimize patient-specific and patient-appropriate FEM. There is no convincing mathematical correlation between grey-level pixel/voxel intensity values, HU, BMD, and elastic modulus in the form of a sliding scale or a log table currently available that can be predictably applied directly with confidence in clinical practice for *patient-specific* and *patient-appropriate* surgical applications.

8.0 Finite element method and finite element modeling

8.1 Why finite element modeling?

In structural engineering, the in-silico (computer-based referring to silicon) assessment of the structures is a well-established technique by applying the finite element method. Since the early 1970s, it has been increasingly applied to study the competency of surgical implants in conjunction with experimental biomechanics(Brekelmans et al., 1972; Huiskes & Chao, 1983). More recently the role of the FE model has been extended to patient-specific surgical planning. FEM as an engineering tool can be used easily to analyze any complex biological structure that responds to physical laws. Building a physical model, real or virtual, brings an

opportunity to apply engineering principles to biological tissues to understand their mechanical behaviour and extract information for clinical applications. The process allows simulation of near-life deformation of biological materials, both solid and fluid, to the applied mechanical forces on given 3D geometry in-silico.

All biological structures are constructed of multiple extrinsic layers and intrinsic organ systems with their elements arranged in interlacing elastic strings, beams, and struts made up of solid, semisolid, and fluid materials in a variety of configurations giving heterogeneous appearances on radiographic images. Therefore, it becomes necessary that a physical or a virtual model is realistic enough to represent various structures such that both the extrinsic and intrinsic tissues experience corresponding mechanical deformation under mechanical loads. In biomedical engineering, many physical models for biological applications are heuristic models, such as a spring, based on Hooke's law to represent muscles. On the other hand, computer models are based on continuum mechanics to run finite element analyses. The heuristic models are computationally less expensive, but they produce random and inconsistent results. Comparatively, FEM with a higher computational cost is more accurate for intricate multilayered structural anatomy with multiple elements expected to experience large deformation under displacement forces(Ladjal et al., 2013; Zhang et al., 2018). Therefore, the FE modeling permit study of inter-relationship between different tissues under applied forces (loads) and constraints (boundary conditions) to produce tissue displacement more specifically in *patient-specific* and *patient-appropriate* clinical applications.

8.2 Mesh structure of finite elements

A FE model is constructed by dividing and subdividing a continuous structure into a finite number of finite-size elements(Bro-Nielsen, 1998; Zienkiewicz et al., 2013). Each element can have an infinite degree of freedom under mathematical conditions but is generally limited by finite differential and algebraic equations due to few known finite parameters for clinical applications. The numerical analysis is conducted on the discretized structure, applied discretely on each finite element represented in a mesh either overlaid or embedded within the structure. The deformation or displacement of the structure is recorded as a change in its physical configuration (strain) and a change in its potential energy experienced by each element of the mesh. The FE mesh is a non-overlapping network constructed by arbitrarily dividing a surface and/or intrinsic substance of a solid or fluid into simple geometrical elements like tiles resulting in a tessellation of the space. 2D elements are geometric primitives such as squares, and triangles and in the case of 3D space, the elements can be made-up of cubes, tetrahedrons, hexahedrons, pyramids, or other prismatic shapes. Each vertex (corner) of a polyhedron is represented by a node and has edges and faces shared with other elements in the mesh. The mesh can be purely made of a tetrahedron, hexahedron, or a hybrid of two or more shaped elements. Tetrahedrons are more commonly used for the analysis of medical structures, but hexahedron elements have greater accuracy because they can deform in a lower strain energy milieu under varying conditions(Benzley et al., 1995).

The FE methods based on the mesh can be time-consuming to generate patient-specific FE mesh for analysis where the structural anatomy is intricate(Wittek et al., 2016). In the case of an anatomical structure where there are multiple hard and soft tissue inclusions for FE analysis, only nodes without the connecting elements are preferred to form a standard grid instead of a complete mesh, to calculate stress and strain at the nodes by applying an explicit Lagrangian dynamic algorithm for surgical simulation(Horton et al., 2010).

To perform medical image analysis, the structure of bones is better visualized on CT and soft tissue structures are delineated better with MRI imaging. Before the construction of the FE mesh, the image is segmented digitally or manually to segregate the region of interest. The meshing process begins with the input of extrinsic mesh on the surface of a segmented model as a shell and intrinsic mesh is established as volumetric solid FE mesh from the reconstruction of 2D slices of CT and MRI images into 3D. In a 3D image, the volumetric FE element is represented as a hexahedral voxel. Voxel meshes are practical for the simulation and examination of a structure. Computing time is proportional to the density and geometry of the mesh elements. But quantity and quality of the mesh are important variables to accurately simulate the geometry and increase precision. For refinement of the mesh denser clusters of elements at important sites and sparse ones at others are built into the mesh, and for faster analysis parallel algorithms can be run on graphic processing units (GPU) for numerical solutions. The GPU acts as a co-processor to the central processing unit for executing code run in parallel. GPU with its multi-threaded architecture is designed to compute parallel data with high arithmetic intensity. Further details on FE methods for meshing techniques and automatic mesh creation are beyond the scope of this review. There is

extensive published literature available for interested readers(Giovannelli et al., 2014; Hitschfeld-Kahler, 2005; Keyak et al., 1990; Lorensen & Cline, 1987; Viceconti et al., 1998).

9.0 Clinical consideration of finite element method

The much greater impetus to the application of FE methods has come from improved imaging technology and data analysis capability of desktop computing. This has opened possibilities to design and custom-fit patient-specific implants and the ability to select a *patient-appropriate* implant from the existing stock in a hospital to make better choices and improve outcomes for surgical applications. As FEA is a specialized engineering tool, therefore within the surgical environment the objective of better choices for improved surgical outcomes is only possible if there is a dedicated team of clinical biomechanical engineers(Gandhi, 2022). For a greater understanding of each surgery undertaken by the surgical team the collaboration with the clinical biomechanical engineering team ideally should begin the process of computational modeling at the time of pre-operative planning. It is expected that such an approach not only will improve patient-based outcomes but might reduce the surgical cost to the health provider in terms of time, implant fatigue failure, and pre-selection of the implant to limit in-house stock and even consideration of custom additive manufacturing of an implant or a jig to assist anatomical reconstruction. It is about time that FE analysis techniques are transferred in earnest to clinical practice as a surgical tool rather than continue to be an experimental engineering method. There are advocates for "patient-specific" surgical application of FEM now for more than a decade(Neal & Kerckhoffs, 2009; Poelert et al., 2013; Viceconti et al., 2006).

9.1 The practice of finite element modeling and analysis

The essential parameters for *patient-specific* FE modeling of the skeleton include image-based 3D modeling of the bone to acquire its surface characteristics, bone geometry, and material properties of the indexed section of the bone segment; *patient-appropriate* physiological and pathological activity-based loads, and boundary conditions. In the case of the thoracic cage, whenever possible it is important to include fascio-cutaneous soft tissues, adipose tissues, breasts, muscles, tendons, articular cartilages, capsules, and ligaments to complete *patient-specific* model requirements. Include viscoelastic and anisotropic behaviour, elastic modulus, and Poisson's ratio representing material properties of all the soft tissues acting on the skeletal segment of the regional anatomy. The reconstruction of 3D images from 2D radiographic multiple views can be a cost-effective and safe technique in daily surgical practice. To achieve the goals of *patient-specific* engineering of the bone-implant synthesis, any population-based and labour-intensive segmentation techniques requiring a *priori* knowledge for bone modeling, selection of non-*patient-specific* bone material properties from the literature for FE analysis, application of non-patient-appropriate boundary conditions and forces under clinical conditions are less than ideal.

In most cases, 3D CT image reconstruction is a common diagnostic investigation for surgical management of fractures and MRI for elective orthopaedic surgery. The same applies to most open-heart surgery patients for cardio-pulmonary assessment with CT studies of the chest pre-operatively. It provides an adequate opportunity to acquire a 3D image of the thorax for segmentation and FEM. To reduce the radiation exposure the use of the limited exposure CT technique for 3D *patient-specific* FEM comes with errors during thresholding, filtering noise, and smoothing procedures to recreate new 2D slices(Shim et al., 2007). Manipulation of the image during pre-processing may alter grey-level values, particularly along with the edge pixels and voxels during 3D reconstruction, which would hinder intensity-based segmentation of the anatomy, extraction of material properties, and creation of mesh for FE analysis.

The FE-based bone-implant computational modeling for analysis should preferably be automatic to increase efficiency, reproducibility, and accuracy to enhance surgical procedure outcomes. It should be robustly supported by engineering principles to make the surgical procedure ameliorative and safe to represent *patient-appropriate* loading conditions. An ideal biomechanical thoracic cage FE model is required to avoid making sub-optimal implant choices for the reconstruction of osteochondrotomy of the sternum following open heart and major vessel surgery in the mediastinum to improve patient-based outcomes. The biomechanical model of the thorax should include all the components of the articulated thoracic skeleton including the sternum, the clavicles, all the ribs, the thoracic vertebral column with intervertebral discs, the costovertebral and the costo-

sternal articulations with articular cartilages, costal cartilages, capsules, and ligaments. Also include fasciocutaneous adipose tissue and breasts, intercostal muscles and pectoralis group, diaphragm, and the abdominal wall musculature acting directly on the sternum to optimize the forces acting on the split sternum with all necessary physical constraints applied to each component(Ladjal et al., 2013). Intrathoracic organs and sub-diaphragmatic solid organs such as the liver and spleen do have a significant influence on biomechanics of the thoracic cage and be included in constructing a model for respiratory mechanics(Saadé et al., 2010). To keep administration and computation costs low, once a comprehensive master model is ready, it can be utilized as a framework and modified for registering *patient-specific* variations before or after the segmentation of the images. This can be achieved by applying multilayer parametric solid(Wang et al., 2011) or similar modeling techniques to update patient-specific morphometric parameters of the skeletal elements and soft tissues; followed by *patient-specific* material properties, *patient-appropriate* boundary conditions, and loads to study a set of suitable implants in parallel on a system with multi-threaded GPU.

The true ribs (1-6) lift the sternum anteriorly and cranially, while false ribs (7-10) cause anterior and lateral movements, and floating ribs (11 and 12) posteriorly provide attachments to the paravertebral muscles play significant stabilizing and mechanical role acting like calipers during deep breathing by their circumferential expansile movements. The bucket-handle movements of the false ribs apply considerable force to disrupt the distal part of the reconstructed osteochondrotomy of the sternum in the early postoperative period(Dasika et al., 2003). Both the compartments of the trunk, the thoracic cage and the abdominal cavity with mobile piston-like action of the diaphragm assist ventilation under varying physiological and pathological conditions(Wade, 1954; Ward et al., 1992). Obesity has a noteworthy effect on the physiology of breathing by affecting respiratory compliance due to increased weight on the thoracic cage and abdomen to alter the biomechanics of the thoracic cage and diaphragm(Luce, 1980; NAIMARK & CHERNIACK, 1960). Therefore, for the selection of an ameliorative implant, a 3D biomechanical model of the thoracic skeleton including all the soft tissues responsible for its mechanical stability, kinematics, and *patient-appropriate* forces are important.

In women, the breasts form an integral part of the thoracic cage anatomy and have significant mechanical influence due to their weight and geometry. Therefore, it is appropriate to include them when constructing a FE model(García et al., 2018) for bone-implant interface analysis of osteochondrotomy of the sternum. Normally, the base of the breasts spanning an area between the second to the sixth rib vertically, and the lateral border of the sternum to the anterior axillary line horizontally on either side, weigh 500-1000gm(Grassley, 2002). The breast tissue is suspended by Cooper's ligaments from the pectoral fascia covering the pectoralis major, which in turn is inserted into the ipsilateral half of the sternum(Riggio et al., 2000). The unsupported breasts move relative to fixed points on the chest wall, and the skin boundaries move 25-60% depending on the weight from the resting position with the gait cycle of an individual(Khatam et al., 2015). The weight of the breasts exerts an inferior and lateral cyclic force of 5-15N, 5000 times per day, and exceeds 50N during strenuous activity(Gefen & Dilmoney, 2007). For clinical application average weight of each breast may be estimated from the volume (500ml to 1000ml) and tissue density (0.916g/cm^3 to 1.000g/cm^3)(Choppin et al., 2016) by filling a specially designed comfortably fitting breast volume measuring [1]'surgical brassiere meter' made from non-extensible material, sizes from A, B, C…, and/or 3D MRI to acquire the geometry for FE modeling.

The FE modeling techniques described in the literature utilize statistically averaged values of material properties of the human thoracic skeleton and soft tissue structures derived from experimental biomechanical studies(Gzik-Zroska et al., 2013; Ladjal et al., 2013) if applied to would fail the objectives of *patient-specific* and *patient-appropriate medicine* for surgical application. The loading conditions should be physiological and include pathological loads relevant to co-morbid states and known physical non-standard loads other than activities of daily living in young healthy individuals. To conduct FE analysis for implant fitting, consider the viscoelastic and anisotropic nature of the wet bone to duplicate living conditions, and implant geometry and its material properties to make the analysis *patient-specific* and *patient-appropriate*.

10.0 Finite element-based quantification of the divided sternum

[1] Intellectual property of the author

The morphology and bone geometry of the sternum is simple. The cortico-cancellous structure with a thin cortical shell encloses trabecular struts of varying thickness that confers heterogeneous image intensity gradient equivalent to variable bone density. When the image intensity gradient (grey-level scale) is used to extract the material properties' accurate representation at each of the sternebrae the implant holding the osteochondrotomy of the sternum must also be applied. 3D FE model built by applying tetrahedral solid elements to the cortex captures more accurate results than shell-plate elements(Varghese et al., 2011). The advantage of the 3D FE model is that the hexahedral voxelized mesh is more likely to provide volume-based accurate grey-level values, Hounsfield Units, and bone mineral density to extract elastic modulus at each element for the patient-specific bone properties(Helgason et al., 2008). The bone cortex and trabecular structures should be assigned appropriate material properties based on radiographic intensity gradient without assumptions. Similarly, assign boundary constraints and *patient-appropriate* time-dependent loading conditions during the healing of the re-constructed sternum. The strain and intrinsic stress experienced by the tissues at each voxel element and set of nodes that represent bone-implant construct under native forces reflect the mechanical effect of the chosen implant at the cut-edges of cortico-cancellous osteochondrotomy of the sternum under cyclical loads during healing. Direct physical and intrinsic loads due to persistent muscle tone of major skeletal postural muscles also need to be taken into consideration. Ideally, the boundary conditions applied at the bone-implant interface must exceed the safety factor of three times or more than the expected maximum mechanical loads on the cortical surface of the sternum to assess for notching and initiation of the construct failure(Gandhi, 2019).

The primary objective of FEM is an assessment of implant design that fits the geometry and surface characteristics of the split sternum and optimally maintains opposing interfacial forces until healing is complete. The split anatomy of the sternum can be variable due to normal variations and congenital deformities and the objectives can only be fulfilled either by a customized 3D printed implant of a suitable biomaterial or a readily available implant made of a self-contouring material that would hold the divided verges of the sternum until healing is complete. Seemingly, Stainless steel cerclage wire and similar malleable circumferential implants are the only devices that have the self-contouring ability at the time of application to mold around the shape of the sternum. However, the rectangular cross-section of the sternum and soft tissue interposition at the implant-bone interface prevents uniform moulding of even such devices around the sternum. Frequently, uncontrolled force at the time of their application can lead to mal-reduction, progressive loosening, early fatigue and breakage, and gap development due to unexpected high lateral distraction forces resulting in delayed or non-union. Hence, there is a need for a *patient-specific* and *patient-appropriate* approach to selecting implant design during pre-operative planning. There is little room for population-based statistically determined allometric and anthropometric measurements in elective surgical practice for implant selection. To assess the structural integrity of the reconstructed sternum the computational model must be designed pre-operatively and devices analyzed to become ready for application with the collaborative effort of an experienced clinical biomechanical engineer for an expert surgeon to implement the reported in-silico results. FE analysis is the only method available to carry out a selection of *patient-specific* and *patient-appropriate* implant designs to reconstruct an osteochondrotomy of the sternum.

11.0 Verification and validation of finite element analysis

Verification and validation are essential steps for FEM and FEA before the in-silico results can be transferred to the real world and convince the surgical team to accept the choice of an implant based on stress-strain analysis. The availability of a high-level validation process for surgical implementation effectively and specifically to an individual patient is still unknown, because for the validation process biomechanical experiments are performed either on synthetic bone models or animal and human cadaveric bones. The computer modeling parameters are based on the geometry of 3D CT of the cadaveric bones, generic bone material properties, assumed boundary conditions, and loads for solving variable partial differential equations. According to the American Society of Mechanical Engineers Verification and Validation Standard Committee, *"Guide for the verification and validation in computational solid mechanics"* (ASME V and V-10-2006), the verification process determines that a computational model is an accurate representation of the mathematical model and its solution, and validation process determines the degree to which a computational model is an accurate representation of the intended real-world application. FE method provides approximate solutions to real-world problems because several input

parameters are assumptions. There are uncertainties regarding the choice of software, type of finite elements, mesh density, and refinement. There can be mathematical errors during the iteration process, and errors in applying boundary and load conditions. All these factors can add up to have a cumulative effect, particularly when the FEA study is time-dependent, and compared to experimental and past literature data for validation.

Currently, the best approach for *patient-specific* computer modeling is to acquire bone geometry from the 3D CT reconstruction of the index bone segment for surgical intervention. Adopting reliable segmentation techniques, extracting true native bone material properties from patients' 3D image grey-level intensities, *patient-specific* and *patient-appropriate* boundary conditions and loads in-silico FEM and FEA for clinical application can be an intense exercise to execute without the help of a dedicated clinical biomechanical engineering team. Although, during FEA the reconstructed 3D sternum within the thoracic cage model can be cyclically loaded to simulate respiratory movements, cough episodes, and other forces that may act on the healing sternum and a set of implants. But still, what is impossible is to precisely embed physiological and pathological parameters and risk factors, and time-dependent metabolic and progressive tissue healing processes into well-established engineering methods. At present, establishing and assuring one hundred percent safety of in-silico modeling and analysis for the selection of an implant can be difficult to recommend with confidence without practicing the finite element method routinely for long-term surgeon experience to help develop trust in FEM and FEA. It does not mean that the process is impossible. It invites interested practicing scientists to come together without inertia yet remain within the goals of patient safety and outcome.

12.0 Discussion

The "single-patient" is a statistical term, which refers to the n-of-1 trial methodology where a treatment plan is specifically developed for a single patient that is appropriate only for that person, precisely defining the *'patient-specific and patient-appropriate medicine'* in clinical practice. As the patient is the sole beneficiary of this intense investigative exercise, therefore, it begins with the surgical workup from the time of the first clinical encounter with a patient to the time he or she receives the expected outcome in a minimal time in a cost-effective manner. To successfully fulfill such objectives of reconstructing a fracture or an osteotomy the knowledge of bone geometry, bone mineral density, the elastic modulus of the soft and hard tissues, boundary conditions, and loads applied to a skeletal segment are key factors for exercising *patient-specific* and *patient-appropriate* implant selection based on the finite element method. In case multiple implants or a variety of implants are required to reconstruct a skeletal segment such as the sternum, it requires extraction of localized bone mineral density distribution based on pixel grey-level values without the alteration of original image characteristics to calculate mechanical properties at each one of the sternebrae for the fixation of one or more types of implants. As most of the patients requiring osteochondrotomy of the sternum present with comorbidities that variously affect bone healing under different boundary and loading conditions, it also demands modeling the soft tissue envelope including major muscle groups affecting articulated skeletal segments associated with the index segment and their native mechanical properties for FEA.

As of now, there is no standardization of imaging technologies between each other for the acquisition of equivalent pixel grey-level values for medical images based on soft and hard tissue characteristics. Similarly, there are no reliable power laws to extract true material properties from BMD to calculate *patient-specific* mechanical properties for surgical applications under conditions of *patient-appropriate* physiology and pathology. Other than averaged HU/CT number applied at each node of FE mesh none of the image modalities provide in-vivo true BMD based on microarchitecture at a specific site. A large point x-ray source of a standard CT machine produces geometrical backtracking of the photon path through the samples to cause shadows and blurring making it unreliable for quantitative CT procedures. Whereas micro-CT produces a sharper x-ray beam for accurate quantitative measurements of bone mineral content(Landis & Keane, 2010; Teo et al., 2006). For quantitative CT measurements, a calibration curve is generated each time by exposing phantoms of various known densities. And, from this calibration curve, each voxel grey-level value of the 3D bone sample is converted to bone mineral densities. Bone mineral content at the micro-level can also be extracted by scanning the surface of bone samples with a scanning electron microscope(Roschger et al., 1995). The high-speed focused beam of electrons elastically interacts with the bone sample. The reflected scattered electrons from atoms of higher atomic numbers are recorded as brighter grey-level images and one with a lower atomic number is darker. The

intensity of backscattered electron proportional to atomic numbers of various atoms in each bone specimen provides a spectrum of grey-level values(Bereshiem et al., 2019). The grey-level values can be used to calculate apparent bone density and material properties by applying Morgan's law or similar material power laws.

Animal reproduction of its' own 'kind' is a gross example of self-similarity from the fusion of non-similar elements, at least in appearance! Once past the stem cell self-similarity upon functional cell differentiation its self-similarity is lost and then cell-type self-similarity follows to have an independent organization within the entire animal structure of dissimilarities. Self-similarity in chirality (the right and left-handedness and physical non-superimposition) of Laevo- and Dextro-rotation as seen in chemical isomers also occur during embryonic development of animals that leads to the development of non-superimposing bilateral structures, with exception of mid-sagittal axial structures such as the sternum, for attaining optimal mechanical strength and co-ordination of functions in organisms from the nanoscale to macroscale levels, with likely variations at intermediate levels due to extrinsic influences. A rope consisting of multiple fibres twisted into yarn, and then multiple bundles of yarn wound together provide structural and functional requirements to attain its' tensile strength rather than compressive strength and is a simple everyday example of hierarchical "Fractal" and "Chirality." Another interesting example is folding any A-size paper sheet seven times (maximum structural paper folding hierarchy) over itself will not fold any further achieving optimal mechanical strength and functionality that can be used as a fracture-splint safely! There are nine levels of chirality of bone structure from atomic to macroscale.

Similarly, the hierarchical "fractal-like" organization(Reznikov et al., 2018) and chirality(Zhou et al., 2022) of bone based on the concept of Mandelbrot's "Fractal" refers to self-similar structural elements organized in a specific repetitive manner at all levels. At the macroscale and microscale level "Fractal index" or "Fractal dimension,"(Camargo et al., 2016; Harrar & Hamami, 2008) as a ratio or Fractal box-counting refers to the 'shape' and measure of the open and closed cells (lacunae) to the thickness of enclosing columnar and plate-like trabeculae to describe bone density is in two dimensions rather than three dimensions. Biologically, the observed dynamic qualitative and quantitative change in the dimension of trabeculae and their geometric arrangement within a section of a bone segment during remodeling is well described by [2]Wolff's Law, Heuter-Volkman's Law, and piezoelectric charge in response to the local and global forces acting on it in compression and tension. However, these biological laws ignore the chirality of bone tissue to torque and the influence of interfacial shear between various elements in response to the applied load, which may have a significant impact on the fracture healing tissues and the development of fracture geometry at the time of injury. Since in engineering terms the trabeculae under multitudinous forces remodel for maximum material strength and stiffness, a variety of geometrical shapes of the intertrabecular lacunae is the result of biological minimalization of weight and material optimization process for minimization of energy consumption. Thus, geometrical shapes of the lacunae can hardly be approximated to be self-similar to truly follow the concept of Mandelbrot's Fractal, which simply said is akin to self-similar zoom-in zoom-out or making multiple micro-sized copies supposed to be self-similar of the original image, whereas measured "Fractal dimension" is a set of calculated mathematical values recommended for clinical application.

Certainly, there will be load-dependent varyingly distributed changes in the dimension of the lacunae due to thickening and thinning, and loss of trabeculae leading to a greater dissimilitude is said to have a geometrical affinity has been exploited as a "Fractal dimension." At a specific section of a bone segment under study, there is a significant correlation between "Fractal dimension" and pixel grey level, but no correlation to bone density(Camargo et al., 2016). Therefore, the terms "Fractal index or Fractal dimension" is best avoided to describe bone density and osteoporosis for clinical applications. As the triangle is the simplest of all the geometrical primitives the Mandelbrot's Fractals are exemplified as a homogeneous Sierpinski triangle **(**Fig. 7B

[2] According to the Wolff's law increasing mechanical stress leads to significant bone mass gain and vice-versa and the Heuter-Volkman's law suggests that compression forces inhibit growth and tensile forces stimulate growth in an immature skeleton. Like the Wolff's law, piezoelectricity on the compression side generates electronegative charge to stimulate osteoblasts laying new bone and on the tensile side electropositive charge stimulate osteoclasts leading to resorption.

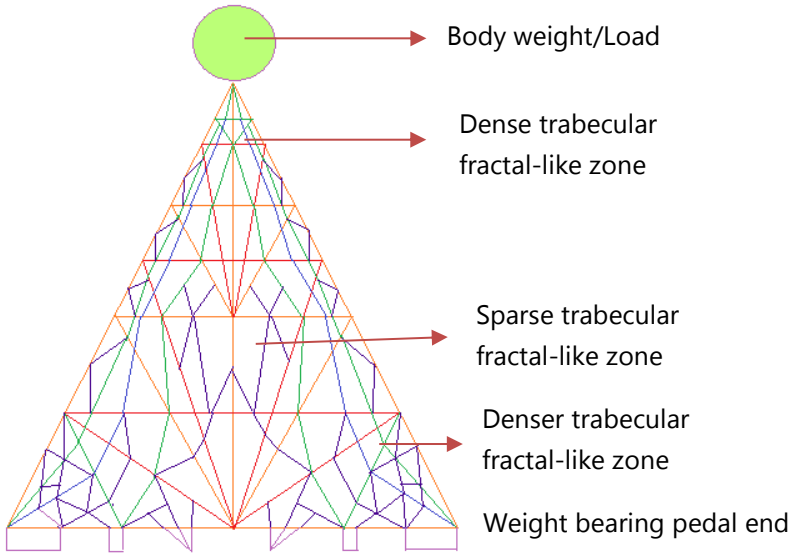

A.

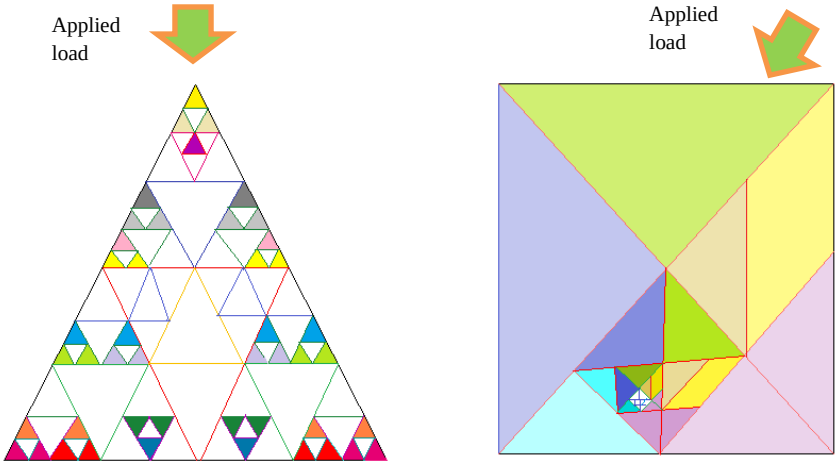

B.

C.

Figure 7 – **A.** A two-dimensional hypothetical representation of the trabecular structure of metaphyseal bone depicting two or more types of geometric primitives as "Fractals," which is not so dissimilar to a **B.** (right) Chinese tangram showing a variety of primitive geometric shapes and (left) a Sierpinski triangle**. C.** An example of "fractal-like" organization at the macroscale level, does not appear to be so self-similar as

repeating geometric shapes of the lacunae. The variability in the load-directed distribution of the trabeculae and geometric shapes of the lacunae can be seen in this section of the neck of a femur. There is a meaningful biological order even in what may appear to be chaotic, in response to applied loads!

left**),** described much before the "Fractals," does not lend itself well to the heterogeneous two-and three-dimensional geometry of intertrabecular lacunae **(**Fig. 7C**)** to be called "Fractals" in its true sense. Instead, it may be better represented by manifold variegated prismatic and/or spheroidal shapes and arranged in response to the likely distribution of the applied load as shown in **(**Fig. 7A**)** or a Chinese tangram (Fig. 7B right**)**. Whether the term "Fractal" compounded with another scientific term applies to trabecular-lacunar architecture or not needs further elucidation, particularly for *patient-specific* applications, if at all, to assess bone density to establish optimal fixation of a surface implant via screw thread-bone interface in the metaphyseal section of a bone segment. In this regard, the orthopaedic community has followed the right and left-handedness and surface bone chirality features to adopt right and left, and pre-contoured fracture fixation systems. It is a matter of becoming cognizant of the unique anatomical position of the sternum as an important mid-sagittal axial structure that defies several *patient-specific* and *patient-appropriate* requirements when it comes to reconstructing the osteochondrotomy of the sternum.

Initially, *patient-specific* BMD can be measured retrospectively by performing scanning electron microscopy(Roschger et al., 1998) on bone samples taken intra-operatively from the sterna for comparison to in-silico pre-operative results based on image intensity to build data for the validation of process in a longitudinal study as a *posteriori* for the validation of future FEA. A rectangular cortico-cancellous bone sample measuring 4 x 2 x 4 mm can be taken from the osteotomy edge of the sternum with the help of a specially designed non-crushing instrument during surgery at the level of each sternebra and subjected to quantitative micro-CT to directly measure bone density from image intensities. No special time-consuming sample preparation is needed for micro-CT imaging. Therefore, the same intact samples can be further processed for scanning electron microscopy to corroborate the bone density results of the bone sample obtained with micro-CT image intensity. These intensities can be further compared to the standardized pre-operative plain radiographic and/or CT image intensity gradient at the corresponding sites of the same patient sternum to calculate tissue material properties to develop a sliding scale (relationship between bone mineral density, grey-scale level values, and elastic modulus) for the future reference. The sliding scale data can then be applied to the new patients in the future to confer equivalent *patient-specific* material properties improving the results of their stress-strain FE analysis, in turn expecting a more realistic outcome of the tested implant.

The most important step is to first develop a hospital-based dedicated team of clinical biomechanical engineers to undertake these kinds of activities as hospital practitioners, initially in tertiary centres at the regional level. Later, with improvement in technology and skills, increasing success in implant predictability and trust based on engineer-surgeon experience, the practice can be expanded to satellite centres or even subcontracted to federally approved facilities equipped with additive manufacturing. If the efforts to develop "patient-specific" solutions are kept at the research and experimental level in engineering laboratories, they will never materialize into therapeutic application in daily practice. An earnest cost analysis is only possible when there is a team in operation to undertake such studies.

10.0 Conclusion

Building a bridge between engineering and surgical principles and a trusting relationship between two diverse teams can never be easy. Initially, the experience of the surgeon may outweigh the FE analysis performed by the clinical biomechanical engineer based on available data, until both teams have sufficient opportunity and experience of patient-based and surgeon-based evidence built on the practice of *patient-specific* and *patient-appropriate medicine*. In the case of re-synthesis of osteochondrotomy of the sternum, if FE analysis of six or more figure-of-zero cerclage wires produces results like other tested commercially available advanced implants, it is preferable to apply cerclage wires to keep the cost down, for ease of application. Otherwise, preference should be given to the next most ameliorative implant to reconstruct the sternum following the tenets of *patient-appropriate medicine*(Gandhi, 2019).

Over time a local library of new patients treated based on in-silico FEA will help build a hierarchy of a variety of ameliorative implants. Then post-operative patient-based outcome scores can be tallied with the objective FEM and FEA score system to corroborate and validate the results of the FEA in future instances to generate greater confidence. Above all, it is a matter of providing sufficient science-based trust to make surgical choices to make the patients believe and sign well-informed consent for surgery under conditions of in-silico analysis. The concept of in-silico, n-of-1trial to take the study of *'patient-specific* and *patient-appropriate medicine'* further has been explored in the next part of this series.

Conflict of interest: The author declares that he has no conflicts of interest.

Funding: The study was unfunded.

References:

Adams, J. E. (2009). Quantitative computed tomography. *European Journal of Radiology*, *71*, 415–424. https://doi.org/doi:10.1016/j.ejrad.2009.04.074

Aubin, C. É., Dansereau, J., Parent, F., Labelle, H., & De Guise, J. A. (1997). Morphometric evaluations of personalised 3D reconstructions and geometric models of the human spine. *Medical and Biological Engineering and Computing*. https://doi.org/10.1007/BF02510968

Battistelli, J. M., & Anselem, B. (1993). [Echography in injuries of costal cartilages]. *Journal de Radiologie*.

Benzley, S. E., Perry, E., Merkley, K., Clark, B., & Sjaardema, G. (1995). A Comparison of All-Hexahedral and All-Tetrahedral Finite Element Meshes for Elastic and Elasto-Plastic Analysis. *4th International Meshing Roundtable, Sandia National Laboratories*. https://doi.org/10.1.1.70.392

Bercoff, J., Tanter, M., & Fink, M. (2004). Supersonic shear imaging: A new technique for soft tissue elasticity mapping. *IEEE Transactions on Ultrasonics, Ferroelectrics, and Frequency Control*. https://doi.org/10.1109/TUFFC.2004.1295425

Bereshiem, A. C., Pfeiffer, S. K., Grynpas, M. D., & Alblas, A. (2019). Use of backscattered scanning electron microscopy to quantify the bone tissues of midthoracic human ribs. *American Journal of Physical Anthropology*. https://doi.org/10.1002/ajpa.23716

Brekelmans, W. A. M., Poort, H. W., & Slooff, T. J. J. H. (1972). A new method to analyse the mechanical behaviour of skeletal parts. *Acta Orthopaedica*, *43*(5), 301–317. https://doi.org/10.3109/17453677208998949

Brody, W. R., Butt, G., Hall, A., & Macovski, A. (1981). A method for selective tissue and bone visualization using dual energy scanned projection radiography. *Medical Physics*. https://doi.org/10.1118/1.594957

Bro-Nielsen, M. (1998). Finite element modeling in surgery simulation. *Proceedings of the IEEE*. https://doi.org/10.1109/5.662874

Budoff, M. J., Hamirani, Y. S., Gao, Y. L., Ismaeel, H., Flores, F. R., Child, J., Carson, S., Nee, J. N., & Mao, S. (2010). Measurement of thoracic bone mineral density with quantitative CT. *Radiology*. https://doi.org/10.1148/radiol.10100132

Camargo, A. J., Côrtes, A. R. G., Aoki, E. M., Baladi, M. G., Arita, E. S., & Watanabe, P. C. A. (2016). Analysis of Bone Quality on Panoramic Radiograph in Osteoporosis Research by Fractal Dimension. *Applied Mathematics*. https://doi.org/10.4236/am.2016.74035

Carter, D. R., & Hayes, W. C. . (1977). The Compressive Behavior Porous of Bone Structure as a Two-Phase. *The Journal of Bone and Joint Surgery*. https://doi.org/10.1007/978-1-4471-5451-8_116

Choi, Y. W., Im, J. -G, Song, C. S., & Lee, J. S. (1995). Sonography of the costal cartilage: Normal anatomy and preliminary clinical application. *Journal of Clinical Ultrasound*. https://doi.org/10.1002/jcu.1870230407

Choppin, S. B., Wheat, J. S., Gee, M., & Goyal, A. (2016). The accuracy of breast volume measurement methods: A systematic review. In *Breast*. https://doi.org/10.1016/j.breast.2016.05.010

Consensus development conference: Diagnosis, prophylaxis, and treatment of osteoporosis. (1993). *The American Journal of Medicine*. https://doi.org/10.1016/0002-9343(93)90218-e

Dalstra, M., Huiskes, R., Odgaard, A., & van Erning, L. (1993). Mechanical and textural properties of pelvic trabecular bone. *Journal of Biomechanics*. https://doi.org/10.1016/0021-9290(93)90014-6

Dansereau, J., & Stokes, I. A. F. (1988). Measurements of the three-dimensional shape of the rib cage. *Journal of Biomechanics*. https://doi.org/10.1016/0021-9290(88)90127-3

Dasika, U. K., Trumble, D. R., & Magovern, J. A. (2003). Lower sternal reinforcement improves the stability of sternal closure. *Annals of Thoracic Surgery*, *75*(5), 1618–1621. https://doi.org/10.1016/S0003-4975(02)04988-3

Dobbins, J. T., & McAdams, H. P. (2009). Chest tomosynthesis: Technical principles and clinical update. *European Journal of Radiology*. https://doi.org/10.1016/j.ejrad.2009.05.054

Dobbins, J. T., McAdams, H. P., Godfrey, D. J., & Li, C. M. (2008). Digital tomosynthesis of the chest. In *Journal of Thoracic Imaging*. https://doi.org/10.1097/RTI.0b013e318173e162

Dobbins, J. T., McAdams, H. P., Sabol, J. M., Chakraborty, D. P., Kazerooni, E. A., Reddy, G. P., Vikgren, J., & Bath, M. (2017). Multi-institutional evaluation of digital tomosynthesis, dual-energy radiography, and conventional chest radiography for the detection and management of pulmonary nodules. *Radiology*. https://doi.org/10.1148/radiol.2016150497

Dworzak, J., Lamecker, H., Von Berg, J., Klinder, T., Lorenz, C., Kainmüller, D., Seim, H., Hege, H. C., & Zachow, S. (2010). 3D reconstruction of the human rib cage from 2D projection images using a statistical shape model. *International Journal of Computer Assisted Radiology and Surgery*. https://doi.org/10.1007/s11548-009-0390-2

Fenster, A., & Downey, D. B. (1996). 3-D ultrasound imaging: A review. In *IEEE Engineering in Medicine and Biology Magazine*. https://doi.org/10.1109/51.544511

Forman, J. L., De Dios, E. D. P., Dalmases, C. A., & Kent, R. W. (2010). The contribution of the perichondrium to the structural mechanical behavior of the costal-cartilage. *Journal of Biomechanical Engineering*. https://doi.org/10.1115/1.4001976

Forman, J. L., & Kent, R. W. (2011). Modeling costal cartilage using local material properties with consideration for gross heterogeneities. *Journal of Biomechanics*. https://doi.org/10.1016/j.jbiomech.2010.11.034

Gandhi, H. S. (2019). Rationale and options for choosing an optimal closure technique for primary midsagittal osteochondrotomy of the sternum. Part 3: Technical decision making based on the practice of patient-appropriate medicine. *Critical Reviews in Biomedical Engineering*. https://doi.org/10.1615/CritRevBiomedEng.2019026454

Gandhi, H. S. (2022). A Comprehensive Review of Computer Vision Techniques to Interest Physicians and Surgeons, Role of A Clinical Biomechanical Engineer in Pre-Operative Surgical Planning, And Preamble To HSG-Amoeba, A New Concept of Biomedical Image Modeling Technique. *International Journal of Computer and Technology*, *Vol. 22 (2022)*, 1–49. https://doi.org/10.24297/ijct.v22i.9219

García, E., Diez, Y., Diaz, O., Lladó, X., Martí, R., Martí, J., & Oliver, A. (2018). A step-by-step review on patient-specific biomechanical finite element models for breast MRI to x-ray mammography registration. In *Medical Physics*. https://doi.org/10.1002/mp.12673

Gefen, A., & Dilmoney, B. (2007). Mechanics of the normal woman's breast. *Technology and Health Care*.

Gennisson, J. L., Deffieux, T., Macé, E., Montaldo, G., Fink, M., & Tanter, M. (2010). Viscoelastic and anisotropic mechanical properties of in vivo muscle tissue assessed by supersonic shear imaging. *Ultrasound in Medicine and Biology*. https://doi.org/10.1016/j.ultrasmedbio.2010.02.013

GEOFF DOUGHERTY. (2009). *Digital Image Processing for Medical Applications*. Cambridge University Press.

Giovannelli, L., Marco, O., Navarro, J. M., Giner, E., & Ródenas, J. J. (2014). Direct creation of finite element models from medical images using Cartesian grids. *Computational Vision and Medical Image Processing IV - Proceedings of Eccomas Thematic Conference on Computational Vision and Medical Image Processing, VIPIMAGE 2013*.

Glaser, D. A., Doan, J., & Newton, P. O. (2012). Comparison of 3-dimensional spinal reconstruction accuracy: Biplanar radiographs with eos versus computed tomography. *Spine*. https://doi.org/10.1097/BRS.0b013e3182518a15

Goswami, B., & Kr., S. (2015). 3D Modeling of X-Ray Images: A Review. *International Journal of Computer Applications*. https://doi.org/10.5120/ijca2015907566

Grassley, J. S. (2002). Breast reduction surgery. What every woman needs to know. *AWHONN Lifelines / Association of Women's Health, Obstetric and Neonatal Nurses*. https://doi.org/10.1111/j.1552-6356.2002.tb00088.x

Gzik-Zroska, B., Wolański, W., & Gzik, M. (2013). Engineering-aided treatment of chest deformities to improve the process of breathing. *International Journal for Numerical Methods in Biomedical Engineering*. https://doi.org/10.1002/cnm.2563

Harrar, K., & Hamami, L. (2008). The fractal dimension correlated to the bone mineral density. *WSEAS Transactions on Signal Processing*.

Helgason, B., Perilli, E., Schileo, E., Taddei, F., Brynjólfsson, S., & Viceconti, M. (2008). Mathematical relationships between bone density and mechanical properties: A literature review. In *Clinical Biomechanics*. https://doi.org/10.1016/j.clinbiomech.2007.08.024

Hitschfeld-Kahler, N. (2005). Generation of 3D mixed element meshes using a flexible refinement approach. *Engineering with Computers*. https://doi.org/10.1007/s00366-005-0306-x

Horton, A., Wittek, A., Joldes, G. R., & Miller, K. (2010). A meshless Total Lagrangian explicit dynamics algorithm for surgical simulation. *International Journal for Numerical Methods in Biomedical Engineering*. https://doi.org/10.1002/cnm.1374

Hosseinian, S., & Arefi, H. (2015). 3D reconstruction from multi-view medical X-ray images - Review and evaluation of existing methods. *International Archives of the Photogrammetry, Remote Sensing and Spatial Information Sciences - ISPRS Archives*. https://doi.org/10.5194/isprsarchives-XL-1-W5-319-2015

Huang, Y., Zhou, Q., Wang, S. C., Nie, B. B., & Holcombe, S. A. (2019). An anatomic indexing system for costal cartilage and its application in calcification representation in finite-element human body models. *Conference Proceedings International Research Council on the Biomechanics of Injury, IRCOBI*.

Huiskes, R., & Chao, E. Y. S. (1983). A survey of finite element analysis in orthopedic biomechanics: The first decade. *Journal of Biomechanics*. https://doi.org/10.1016/0021-9290(83)90072-6

Kaufman and Siffert). (2001). Noninvasive Measurement of Bone Integrity. In S. Cowin (Ed.), *Bone Mechanics Handbook* (Second, p. 980). CRC press, Taylor & Francis group.

Kent, D. M., & Hayward, R. A. (2007). Limitations of applying summary results of clinical trials to individual patients: The need for risk stratification. In *Journal of the American Medical Association*. https://doi.org/10.1001/jama.298.10.1209

Keyak, J. H., Lee, I. Y., & Skinner, H. B. (1994). Correlations between orthogonal mechanical properties and density of trabecular bone: Use of different densitometric measures. *Journal of Biomedical Materials Research*. https://doi.org/10.1002/jbm.820281111

Keyak, J. H., Meagher, J. M., Skinner, H. B., & Mote, C. D. (1990). Automated three-dimensional finite element modelling of bone: a new method. *Journal of Biomedical Engineering*. https://doi.org/10.1016/0141-5425(90)90022-F

Khatam, H., Reece, G. P., Fingeret, M. C., Markey, M. K., & Ravi-Chandar, K. (2015). In-vivo quantification of human breast deformation associated with the position change from supine to upright. *Medical Engineering and Physics*. https://doi.org/10.1016/j.medengphy.2014.09.016

Ladjal, H., Shariat, B., Azencot, J., & Beuve, M. (2013). Appropriate biomechanics and kinematics modeling of the respiratory system: Human diaphragm and thorax. *IEEE International Conference on Intelligent Robots and Systems*. https://doi.org/10.1109/IROS.2013.6696623

Landis, E. N., & Keane, D. T. (2010). X-ray microtomography. In *Materials Characterization*. https://doi.org/10.1016/j.matchar.2010.09.012

Laporte, S., Skalli, W., de Guise, J. A., Lavaste, F., & Mitton, D. (2003). A biplanar reconstruction method based on 2D and 3D contours: Application to the distal femur. *Computer Methods in Biomechanics and Biomedical Engineering*. https://doi.org/10.1080/1025584031000065956

Lau, A. G., Kindig, M. W., & Kent, R. W. (2011). Morphology, distribution, mineral density and volume fraction of human calcified costal cartilage. *Acta Biomaterialia*. https://doi.org/10.1016/j.actbio.2010.10.019

Lau, A., Oyen, M. L., Kent, R. W., Murakami, D., & Torigaki, T. (2008). Indentation stiffness of aging human costal cartilage. *Acta Biomaterialia*. https://doi.org/10.1016/j.actbio.2007.06.008

Levinson, S. F., Shinagawa, M., & Sato, T. (1995). Sonoelastic determination of human skeletal muscle elasticity. *Journal of Biomechanics*. https://doi.org/10.1016/0021-9290(94)00173-2

Lorensen, W. E., & Cline, H. E. (1987). Marching cubes: A high resolution 3D surface construction algorithm. *Proceedings of the 14th Annual Conference on Computer Graphics and Interactive Techniques, SIGGRAPH 1987*. https://doi.org/10.1145/37401.37422

Luce, J. M. (1980). Respiratory Complications of Obesity. *Chest*, *78*(4), 626–631. https://doi.org/doi.org/10.1378/chest.78.4.626

Mandelbrot, B. B. (1983). The fractal geometry of nature /Revised and enlarged edition/. *New York*.

McBroom, R. J., Hayes, W. C., Edwards, W. T., Goldberg, R. P., & White, A. A. (1985). Prediction of vertebral body compressive fracture using quantitative computed tomography. *Journal of Bone and Joint Surgery - Series A*. https://doi.org/10.2106/00004623-198567080-00010

Melhem, E., Assi, A., El Rachkidi, R., & Ghanem, I. (2016). EOS® biplanar X-ray imaging: concept, developments, benefits, and limitations. In *Journal of Children's Orthopaedics* (Vol. 10, Issue 1, pp. 1–14). https://doi.org/10.1007/s11832-016-0713-0

Meuwly, J. Y., & Gudinchet, F. (2004). Sonography of the thoracic and abdominal walls. *Journal of Clinical Ultrasound*. https://doi.org/10.1002/jcu.20070

Morgan, E. F., Bayraktar, H. H., & Keaveny, T. M. (2003). Trabecular bone modulus-density relationships depend on anatomic site. *Journal of Biomechanics*. https://doi.org/10.1016/S0021-9290(03)00071-X

Mozaffari, M. H., & Lee, W. S. (2017). Freehand 3-D Ultrasound Imaging: A Systematic Review. In *Ultrasound in Medicine and Biology*. https://doi.org/10.1016/j.ultrasmedbio.2017.06.009

Mullender, M., Van Rietbergen, B., Rüegsegger, P., & Huiskes, R. (1998). Effect of mechanical set point of bone cells on mechanical control of trabecular bone architecture. *Bone*. https://doi.org/10.1016/S8756-3282(97)00251-2

Murakami, D., Kobayashi, S., Torigaki, T., & Kent, R. (2006). Finite element analysis of hard and soft tissue contributions to thoracic response: sensitivity analysis of fluctuations in boundary conditions. *Stapp Car Crash Journal*.

NAIMARK, A., & CHERNIACK, R. M. (1960). Compliance of the respiratory system and its components in health and obesity. *Journal of Applied Physiology*.

Neal, M. L., & Kerckhoffs, R. (2009). Current progress in patient-specific modeling. *Briefings in Bioinformatics*, *11*(1), 111–126. https://doi.org/10.1093/bib/bbp049

Nicholson, J. A., Tsang, S. T. J., MacGillivray, T. J., Perks, F., & Simpson, A. H. R. W. (2019). What is the role of ultrasound in fracture management? *Bone and Joint Research*. https://doi.org/10.1302/2046-3758.87.BJR-2018-0215.R2

Oyen, M., Murakami, D., & Kent, R. (2005). Mechanical Characterization of Costal Cartilage. *33rd International Workshop of Injury Biomechanics Research*.

Poelert, S., Valstar, E., Weinans, H., & Zadpoor, A. A. (2013). Patient-specific finite element modeling of bones. In *Proceedings of the Institution of Mechanical Engineers, Part H: Journal of Engineering in Medicine*. https://doi.org/10.1177/0954411912467884

Prager, R. W., Gee, A., & Berman, L. (1999). Stradx: Real-time acquisition and visualization of freehand three-dimensional ultrasound. *Medical Image Analysis*. https://doi.org/10.1016/S1361-8415(99)80003-6

Rajulu, S Corner, B. (2013). 3D Surface Scanning. In R. Goonetilleke (Ed.), *The science of footwear*. CRC press.

Reeves, T. E., Mah, P., & McDavid, W. D. (2012). Deriving Hounsfield units using grey levels in cone beam CT: A clinical application. *Dentomaxillofacial Radiology*. https://doi.org/10.1259/dmfr/31640433

Reinhard, K. (2014). Cameras, Coordinates, and Calibration. In K. Reinhard (Ed.), *Concise Computer Vision. An Introduction into Theory and Algorithms* (pp. 215–242). Springer-Verlag.

Rejtarová, O., Slízová, D., Smoranc, P., Rejtar, P., & Bukac, J. (2004). Costal cartilages--a clue for determination of sex. *Biomedical Papers of the Medical Faculty of the University Palacký, Olomouc, Czechoslovakia*. https://doi.org/10.5507/bp.2004.050

Reznikov, N., Bilton, M., Lari, L., Stevens, M. M., & Kröger, R. (2018). Fractal-like hierarchical organization of bone begins at the nanoscale. *Science*, *360*(6388).

Riggio, E., Quattrone, P., & Nava, M. (2000). Anatomical study of the breast superficial fascial system: The inframammary fold unit. *European Journal of Plastic Surgery*. https://doi.org/10.1007/s002380000163

Roschger, P., Fratzl, P., Eschberger, J., & Klaushofer, K. (1998). Validation of quantitative backscattered electron imaging for the measurement of mineral density distribution in human bone biopsies. *Bone*. https://doi.org/10.1016/S8756-3282(98)00112-4

Roschger, P., Plenk, H., Klaushofer, K., Eschberger, J., Grynpas, M. D., Boyde, A., Boyce, T. M., & Skedros, J. G. (1995). A new scanning electron microscopy approach to the quantification of bone mineral distribution: Backscattered electron image grey-levels correlated to calcium K??-line intensities. *Scanning Microscopy*.

Saadé, J., Didier, A. L., Buttin, R., Moreau, J. M., Beuve, M., Shariat, B., & Villard, P. F. (2010). A preliminary study for a biomechanical model of the respiratory system. *VISAPP 2010 - Proceedings of*

the International Conference on Computer Vision Theory and Applications. https://doi.org/10.5220/0002892405090515

Sarvazyan, A., J. Hall, T., W. Urban, M., Fatemi, M., R. Aglyamov, S., & S. Garra, B. (2011). An Overview of Elastography-An Emerging Branch of Medical Imaging. *Current Medical Imaging Reviews*. https://doi.org/10.2174/157340511798038684

Savzyan AP. (2001). *Elastic properties of soft tissue. In Levy, M. et al. Handbook of elastic properties solids, liquids, and Gases. Vol. 3* (M. Levy, H. Bass, & R. Stern, Eds.). Academic Press.

Schileo, E., Dall'Ara, E., Taddei, F., Malandrino, A., Schotkamp, T., Baleani, M., & Viceconti, M. (2008). An accurate estimation of bone density improves the accuracy of subject-specific finite element models. *Journal of Biomechanics*. https://doi.org/10.1016/j.jbiomech.2008.05.017

Selthofer, R., Nikolić, V., Mrčela, T., Radić, R., Lekšan, I., Dinjar, K., & Selthofer-Relatić, K. (2010). Real mineral density of the sternum. *Collegium Antropologicum*.

Shim, V. B., Pitto, R. P., Streicher, R. M., Hunter, P. J., & Anderson, I. A. (2007). The use of sparse CT datasets for auto-generating accurate FE models of the femur and pelvis. *Journal of Biomechanics*. https://doi.org/10.1016/j.jbiomech.2005.11.018

Standring, S. (2008). Gray's Anatomy: The anatomical basis of clinical practice. In *Edinburg. Elsevier Churchill Livingstone*. https://doi.org/10.1017/CBO9781107415324.004

Stewart, J. H., & McCormick, W. F. (1984). A sex- and age-limited ossification pattern in human costal cartilages. *American Journal of Clinical Pathology*. https://doi.org/10.1093/ajcp/81.6.765

Stitzel, J. D., Cormier, J. M., Barretta, J. T., Kennedy, E. A., Smith, E. P., Rath, A. L., Duma, S. M., & Matsuoka, F. (2003). Defining Regional Variation in the Material Properties of Human Rib Cortical Bone and Its Effect on Fracture Prediction. *SAE Technical Papers*. https://doi.org/10.4271/2003-22-0012

Teo, J. C. M., Si-Hoe, K. M., Keh, J. E. L., & Teoh, S. H. (2006). Relationship between CT intensity, micro-architecture and mechanical properties of porcine vertebral cancellous bone. *Clinical Biomechanics*. https://doi.org/10.1016/j.clinbiomech.2005.11.001

Turner, C. H., & Burr, D. B. (2001). Experimental techniques for bone mechanics. In *Bone Mechanics Handbook, Second Edition*.

Varghese, B., Short, D., Penmetsa, R., Goswami, T., & Hangartner, T. (2011). Computed-tomography-based finite-element models of long bones can accurately capture strain response to bending and torsion. *Journal of Biomechanics*. https://doi.org/10.1016/j.jbiomech.2010.12.028

Viceconti, M., Bellingeri, L., Cristofolini, L., & Toni, A. (1998). A comparative study on different methods of automatic mesh generation of human femurs. *Medical Engineering and Physics*. https://doi.org/10.1016/S1350-4533(97)00049-0

Viceconti, M., Testi, D., Taddei, F., Martelli, S., Clapworthy, G. J., & Van Sint Jan, S. (2006). Biomechanics modeling of the musculoskeletal apparatus: Status and key issues. *Proceedings of the IEEE*. https://doi.org/10.1109/JPROC.2006.871769

Vock, P., & Szucs-Farkas, Z. (2009). Dual energy subtraction: Principles and clinical applications. In *European Journal of Radiology*. https://doi.org/10.1016/j.ejrad.2009.03.046

Wade, O. L. (1954). Movements of the thoracic cage and diaphragm in respiration. *The Journal of Physiology*. https://doi.org/10.1113/jphysiol.1954.sp005099

Wang, J., Zhang, H., Lu, G., & Liu, Z. (2011). Rapid parametric design methods for shoe-last customization. *International Journal of Advanced Manufacturing Technology*. https://doi.org/10.1007/s00170-010-3144-y

Ward, M. E., Ward, J. W., & Macklem, P. T. (1992). Analysis of human chest wall motion using a two-compartment rib cage model. *Journal of Applied Physiology*.

Wawrzyk, M., Sokal, J., Andrzejewska, E., & Przewratil, P. (2015). The role of ultrasound imaging of callus formation in the treatment of long bone fractures in children. *Polish Journal of Radiology*. https://doi.org/10.12659/PJR.894548

Wittek, A., Grosland, N. M., Joldes, G. R., Magnotta, V., & Miller, K. (2016). From Finite Element Meshes to Clouds of Points: A Review of Methods for Generation of Computational Biomechanics Models for Patient-Specific Applications. *Annals of Biomedical Engineering*. https://doi.org/10.1007/s10439-015-1469-2

Zhang, J., Zhong, Y., & Gu, C. (2018). Deformable Models for Surgical Simulation: A Survey. In *IEEE Reviews in Biomedical Engineering*. https://doi.org/10.1109/RBME.2017.2773521

Zheng G, Gollmer S, Schumann S, Dong X, Feilkas T, B. M. (2009). A 2D/3D correspondence building method for reconstruction of a patient-specific 3D bone surface model using point distribution models and calibrated X-ray images. *Med Image Anal*, *13*(6). https://doi.org/10.1016/j.media.2008.12.003

Zhou, C., Zhang, X., Ai, J., Ji, T., Nagai, M., Duan, Y., Che, S., & Han, L. (2022). Chiral hierarchical structure of bone minerals. *Nano Research Research*, *15*(2), 1295–1302. https://doi.org/10.1007/s12274-021-3653-z

Zienkiewicz, O., Taylor, R., & Zhu, J. Z. (2013). The Finite Element Method: its Basis and Fundamentals: Seventh Edition. In *The Finite Element Method: its Basis and Fundamentals: Seventh Edition*. https://doi.org/10.1016/C2009-0-24909-9